# Hall Effect

## Measurement Handbook

A Fundamental Tool for Semiconductor
Material Characterization

**Jeffrey Lindemuth, PhD**

Edited by Brad C. Dodrill

# Preface

Edwin Hall, as part of his PhD dissertation, discovered the Hall Effect in 1879[1]. Since this discovery, the Hall effect has become one of the major methods for characterizing electronic carrier transport in semiconducting materials. A measurement of the Hall effect and the resistivity provides a wealth of information such as the carrier density, the mobility of the carriers, and the carrier type. The carrier density is the number of mobile carriers per volume in the material, and for semiconductors, is related to the doping of the semiconductor. The mobility is fundamentally a measure of the velocity of the carriers in the material and is often the most important material parameter measured by the Hall effect. The carrier type tells us if the carriers are holes or electrons. Although this information can be determined by other measurement techniques, the Hall effect is the most prevalent method used to characterize the electronic transport properties of semiconductors.

This guide will start by reviewing methods to measure the resistivity of materials, then the theory of Hall measurements will be discussed. We will review major sources of measurement errors: both intrinsic and geometric sources of errors. We will describe the methods developed to minimize the effects of these errors. As we will see, as the materials of interest have evolved over time, so have the methods to minimize these errors.

# Contents

## Timeline of developments in characterization of electronic materials

In order to describe the useful applications for, and the practical measurements of the Hall effect, it is helpful to provide the following references for historical context, timing, and contributions because this important discovery did not happen in isolation and was significantly enabled by earlier discoveries.
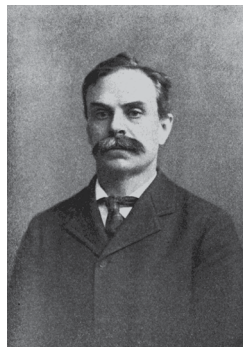


*Edwin H. Hall*

### Instrumentation companies

**1937**    William Hewlett and David Packard founded Hewlett-Packard (HP).

**1937**    Richard Perkin and Charles Elmer founded Perkin Elmer.

**1944**    Floyd W. Bell founded F.W. Bell and developed the first bulk InAs Hall generators and gaussmeters.

**1946**    Howard Vollum, Jack Murdock, Miles Tippery, and Glenn McDowell founded Tektronix, Inc.

**1946**    Joseph F. Keithley founded Keithley Instruments.

**1953**    Jack Mennie and Ernie Porter founded Boonton Electronics.

**1959**    Sir Martin Wood and Audrey Wood (Lady Wood) founded Oxford Instruments.

**1968**    John and David Swartz founded Lake Shore Cryotronics.

**1982**    David Cox, Michael Simmonds, Ronald Sager, and Barry Lindgren founded Quantum Design.

### Discoveries

**1785 — Charles-Augustin de Coulomb**
Published "Premier Mémoire sur l'Électricité et le Magnétisme," ("First Thesis on Electricity and Magnetism") in which he experimentally determined that the force between charged spheres varies as the inverse square of the separation.

**1826 — André-Marie Ampère**
Published mathematical "Théorie des Phénomènes Électro-dynamiques: Uniquement Déduite de l'Expérience," ("Theory of Electrodynamic Phenomena, Uniquely Derived from Experiments") describing Ampère's force law.

**1827 — Georg Ohm**
Published "Die Galvanische Kette, Mathematisch Bearbeitet," ("The Galvanic Circuit Investigated Mathematically") in which his law relating voltage and current was expressed.

**1861/62 — James Clerk Maxwell**
Published theoretical papers titled "On Physical Lines of Force," (in 4 parts). Established as the modern basis of electromagnetic field theory.

**1879 — Edwin Hall** (the focus of this application guide)
Experimentally observed the Hall effect building on Maxwell's theoretical predictions. Defined the interactions between magnetic fields and flowing electric currents.

**1889 — Oliver Heaviside**
Derivation of magnetic force on a moving charged "quantity."

**1891 — George Johnstone Stoney**
Proposed the name Electron for the indivisible charged quantity of Richard Laming (1838).

**1895 — Hendrik Lorentz**
Published "The theory of electrons and its applications to the phenomena of light and radiant heat," refining Maxwell's theories. Determined the force relationships between moving particles in conductors.

**1897 — J.J. Thomson**
Identified the electron as an elementary "Particle" with mass in addition to charge.
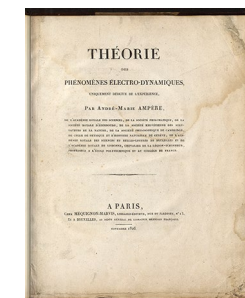
**1900 — Paul Drude**
Published "Zur Elektronentheorie der Metalle," ("On the Electron Theory of Metals") the first classical model of electrical conduction, 73 years after Ohm published the experimental data.

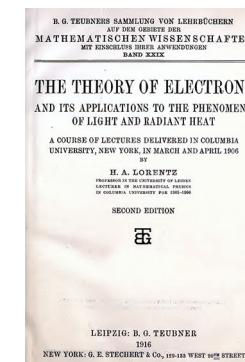**1927 — Arnold Sommerfeld**
Applied Fermi-Dirac statistics to the Drude model of electrons in metals.



*Théorie des Phénomènes Électro-dynamiques: Uniquement Déduite de l'Expérience*



*The theory of electrons and its applications to the phenomena of light and radiant heat*

## Measurement of resistivity

Resistivity is an intrinsic property of a material. The resistivity does not depend on the size or shape of a sample. The extrinsic property measured is the resistance. There are a variety of methods to calculate resistivity from resistance measurements. This section will outline a few of these methods, including Hall bar samples and van der Pauw samples. These are the most important sample geometries used for Hall measurements.

### Ideal one-dimensional (1D) wire

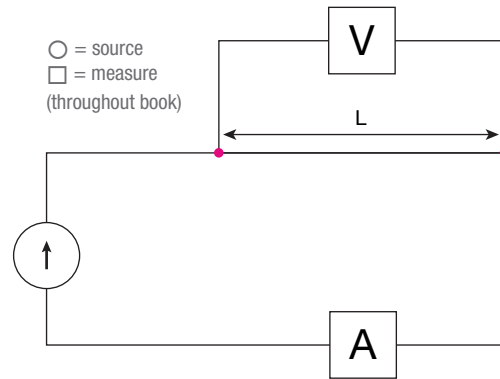We begin with an ideal wire sample of length $L$. This is a mathematical 1D current flow model.



○ = source
□ = measure
(throughout book)

*Figure 1* Circuit for measuring resistivity of a 1D wire.

A source current is applied, and the voltage is measured to determine the resistance of the wire. The current is also independently measured. The current and voltage are related by Ohm's law $(V = IR)$, where $R$ is the resistance of the sample. The 1D resistivity is calculated by $\rho = R/L$ where $L$ is the length of the sample. Note that a physical dimension, in this case the length $L$, is required to calculate the resistivity. In 1D current flow the units of resistivity are $\Omega$/m.

In a real measurement of the voltage and current there can be errors in the measured values due to offsets in the instruments and thermoelectric voltages that arise from contacts between two different materials (e.g., metallic contacts on a semiconductor). These error voltages do not depend on the current and can be corrected by using current reversal.

The measured voltage $(V)$ is $V = IR + V_E$, where $V_E$ is the error voltage. The voltage is measured twice, once with $I_1 = I$ and once with $I_2 = -I$. The two measured voltages are $V_1$ and $V_2$. The resistance of the sample is then calculated by:

$$R = \frac{V_1 - V_2}{I_1 - I_2}$$

This is the slope of the straight line connecting the points $(I_1, V_1)$ and $(I_2, V_2)$ and is called the current reversed resistance or just the resistance.

A 1D wire is a very restrictive model. We can relax this model to include a long thin sample of length $L$ and width $w$. The current is constrained to flow only in the $x$ direction by making the contact on the end as wide as the sample.
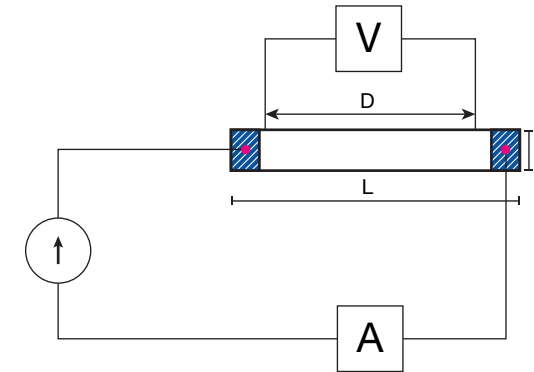
### 1D current flow in a two-dimensional (2D) sample



*Figure 2* A 2D sample with 1D current flow (Hall bar).

The voltage is measured between two contacts a distance $D$ apart. This is to assure that the current flow between the voltage contacts is uniform and only in the direction along the length $L$ of the sample. In this example the model is 2 dimensional, and the resistivity units are $\Omega$. The resistivity $\rho = Rw/D$ where $R$ is the resistance in ohms, and $D$ is the distance between the voltage probes. Note that even though the resistivity and resistance both have units of ohms, they do not have the same value. The resistivity in this case is called the sheet resistivity and is often designated as $\Omega$/square or $\Omega$/sqr or $\Omega$/□ to differentiate it from the resistance. The resistivity is an intrinsic material property and does not depend on the size or shape of the sample used to measure the resistivity. See also the section on 3D resistivity.

### The Hall bar

A practical geometry for measuring resistivity is the structure shown in Figure 3 and is called a Hall bar.
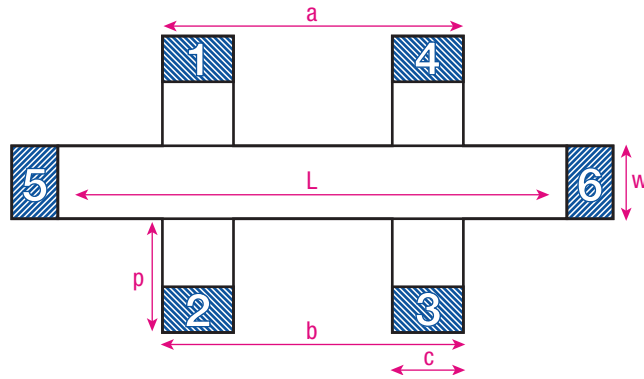


**Figure 3** *A Hall bar for measuring resistivity.*

The Hall bar sample is designed so the current flow from contacts 5 to 6 is 1D. The current source is always connected to contacts 5 and 6. The resistivity is calculated by measuring the voltage between contacts 2 and 3, or contacts 4 and 1. There are two different calculations of the resistivity.

$$\rho_A = \left( \frac{V_{14}(I^+_{56}) - V_{14}(I^-_{56})}{I^+_{56} - I^-_{56}} \right) \frac{w}{a}$$

$$\rho_B = \left( \frac{V_{23}(I^+_{56}) - V_{23}(I^-_{56})}{I^+_{56} - I^-_{56}} \right) \frac{w}{b}$$

$$\rho = \frac{\rho_A + \rho_B}{2}$$

Here and elsewhere in this book the notation *V(I)* means that the voltage *(V)* is a function of current *(I)*.

Placing contacts at the ends of the extended arms reduces the contact-size error to acceptable levels.[2] The following aspect ratio yields small deviations from the ideal: *p ≈ c, c ≤ w/3, L ≥ 4w.*

When the sample is an extended 2D geometry, where the current flow may not be one-dimensional, the problem of converting resistance readings to resistivity is more complicated. In general Poisson's equation, with appropriate boundary conditions and source terms (current source), must be solved to determine the electrical potential throughout the material. The potential difference (voltage) between two contacts, not necessarily the same contacts used for the current source, can be determined. The voltage depends on the electric current and the resistance is the voltage divided by the current. As an example, Figure 4 shows four equally spaced probes at the center of a sample. The probes are far from the edges of the sample. For this geometry, and many similar geometries, there are good approximations to convert the resistance *(V/I)* to resistivity. The book by Schroder[3] provides more detailed information about these methods.
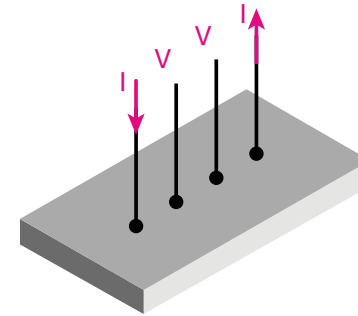
**Figure 4** *An extended 2D sample with contacts for measuring resistivity. This geometry is not suitable for measuring the Hall voltage.*

The previous methods all suffer from the problem that some knowledge of the size of the sample and placement of the probes is required. For instance, in Figure 4 the distance between the probes is needed to convert resistance to resistivity.

In 1958 van der Pauw[4] published his work showing how to determine resistivity from resistance of 2D samples without knowledge of the physical size of the sample. The requirement is that the four contacts are on the edge of the sample and are mathematical point contacts. Also, there can be no holes in the sample (i.e., the sample is simply connected). Later we will address errors from finite contact sizes. A typical van der Pauw structure is illustrated in Figure 5.

The procedure requires two resistance measurements. For instance, the current source is connected between contacts 2 and 1 and the voltage is measured between contacts 3 and 4. The current is reversed to remove thermoelectric voltages and a current reversed resistance is measured. This is denoted as $R_{21,34}$. The current source and voltmeter are rotated to source the current between contacts 3 and 2 and the voltage is measured between contacts 4 and 1. The current is reversed again to remove thermoelectric voltages to obtain a current reversed resistance $R_{32,41}$.

The math to convert these two resistance readings to a resistivity is somewhat complicated, but modern measurement systems can solve the non-linear equation for the factor "*f*" and calculate the resistivity. This resistivity is the sheet resistivity.
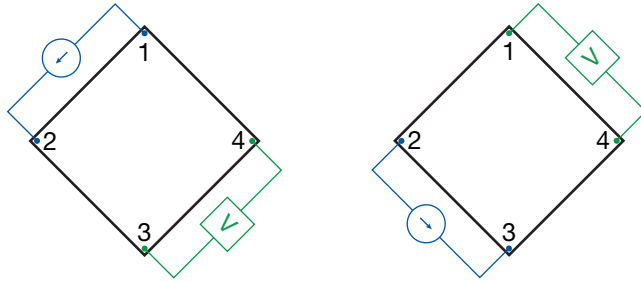
**Figure 5** *A van der Pauw sample showing the connections for resistivity measurements.*

$$R_{21,34} = \frac{V_{34}(I_{21}^+) - V_{34}(I_{21}^-)}{I_{21}^+ - I_{21}^-}$$

$$R_{32,41} = \frac{V_{41}(I_{32}^+) - V_{41}(I_{32}^-)}{I_{32}^+ - I_{32}^-}$$

$$\rho_{sheet}^A = \frac{\pi f}{\ln(2)} \frac{(R_{21,34} + R_{32,41})}{2}$$

Here *f* is the solution to the equation.

$$\frac{q-1}{q+1} = \frac{f \cosh^{-1}(\frac{e^{\frac{ln(2)}{f}}}{2})}{\ln(2)}$$

where

$$q = \frac{R_{21,34}}{R_{32,41}} \; or \; q = \frac{R_{32,41}}{R_{21,34}} \; which \; ever \; is \; larger$$

Figure 6 shows a second set of contacts that can be used in addition to the contacts shown in Figure 5.
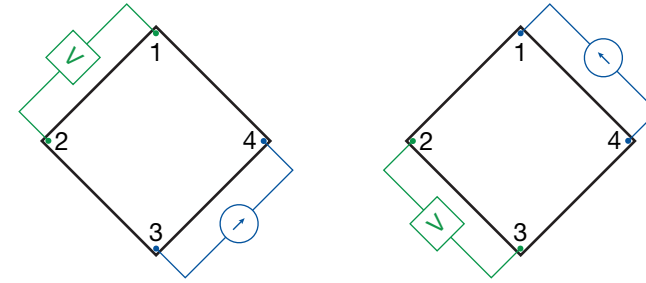


**Figure 6** *A second set of contacts for van der Pauw resistivity.*

$$R_{43,12} = \frac{V_{12}(I_{43}^+) - V_{12}(I_{43}^-)}{I_{43}^+ - I_{43}^-}$$

$$R_{14,23} = \frac{V_{23}(I_{14}^+) - V_{23}(I_{14}^-)}{I_{14}^+ - I_{14}^-}$$

$$\rho_{sheet}^B = \frac{\pi f}{\ln(2)} \frac{(R_{43,12} + R_{14,23})}{2}$$

Here *f* is the solution to this equation

$$\frac{q-1}{q+1} = \frac{f \cosh^{-1}(\frac{e^{\frac{ln(2)}{f}}}{2})}{\ln(2)}$$

where

$$q = \frac{R_{43,12}}{R_{14,23}} \; or \; q = \frac{R_{14,23}}{R_{43,12}} \; which \; ever \; is \; larger$$

The final sheet resistivity is then given by

$$\rho = \frac{\rho_{sheet}^A + \rho_{sheet}^B}{2}$$

Squares and circles are the most common van der Pauw geometries, but contact size and placement can significantly affect measurement accuracy. A few simple cases were treated by van der Pauw.[5] Others have shown that for square samples with sides of length $a$ and square or triangular contacts of size $\delta$ in the four corners, if $\delta/a < 0.1$, then the measurement error is less than 10%.[6] The error is further reduced by placing the contacts on square samples at the midpoint of the sides rather than on the corners.[3] The Greek cross structure shown in Figure 7 has arms that serve to isolate the contacts from the active region. When using the Greek cross sample geometry with $a/c > 1.5$, less than 1% error is introduced in the error of the mobility.[4] A cloverleaf shaped structure like the one shown in Figure 8 is often used for patternable thin films on a substrate. The active area in the center is connected by four pathways to four connection pads around its perimeter. This shape makes the measurement much less sensitive to contact size, allowing for larger contact areas. The contact size affects the voltage required to pass a current between two contacts. Ideal point contacts would produce no error due to contact size but require an enormous voltage to force the current through the infinitesimal contact area.
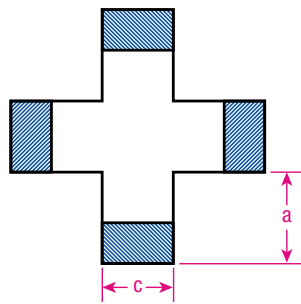


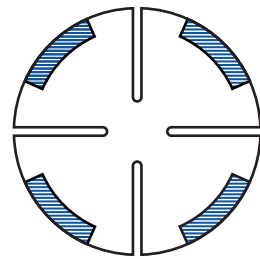**Figure 7**  *Greek cross van der Pauw structure.*

**Figure 8**  *Clover leaf van der Pauw structure.*

For samples that have a thickness $t$, the bulk or 3D resistivity is related to the sheet resistivity by

$$\rho_{bulk} = \rho_{sheet} t$$

The thickness, $t$, should be less than 1 mm.

If comparing the resistivity results among multiple samples, the sheet resistivity can be used for comparison if the thicknesses of all the samples are the same. Otherwise, the bulk resistivity should be used for comparison.

In a conductive material, the moving charged particles that constitute the electric current are called charge carriers. In metals, which are used in wires and other conductors in most electrical circuits, the negatively charged electrons are the charge carriers and are free to move about in the metal with minimal resistance or opposition to their movement. In other materials, notably semiconductors, the charge carriers can be positive or negative (i.e., holes or electrons), depending on the dopant used. Positive and negative charge carriers may even be present coincidentally.

A flow of positive charges (holes) yields the same electric current, and has the same effect in a circuit, as an equal flow of negative charges (electrons) in the opposite direction. Since current can be a flow of either positive or negative charges, or both, a convention is needed for the direction of current that is independent of the type of charge carriers. The direction of conventional current is arbitrarily defined as the same direction that positive charges flow.

Since electrons, the charge carriers in metal wires and most other parts of electric circuits, have a negative charge, they flow in the opposite direction of conventional current flow in an electrical circuit. This is illustrated below. The velocity of the electrons in the figure is negative (opposite to the conventional current flow), while the velocity of positive charge carriers is positive (in the same direction as the conventional current flow).



electron flow

conventional current flow

the ammeter will measure a positive current

A +
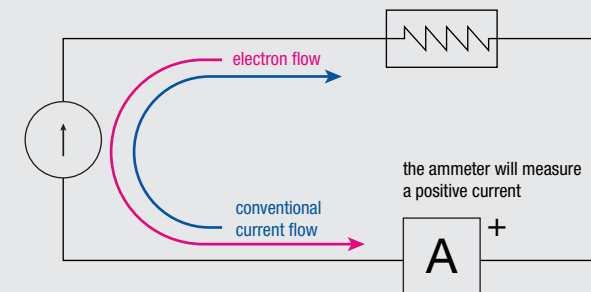
*A positive conventional current flows in the direction of the arrow in the current source. The electron flow is in the opposite direction.*

## Force on a moving charge in a magnetic field

A charge carrier of charge $q$ (signed quantity) moving with velocity $(\vec{v})$ in a magnetic field $(\vec{B})$ will experience a force $(\vec{F})$ from the magnetic field

$$\vec{F} = q\vec{v} \times \vec{B}$$

$\vec{F}$ is the Lorentz force and is perpendicular to both the velocity of the charge carriers and the magnetic field. The charge carrier will rotate around the $B$ field lines as illustrated in Figure 9 with a rotation radius $r = mv/(qB)$ at a frequency $f = qB/(2m)$, where $m$ is the mass of the charge carrier. For electrons in a 1 T field the rotation period is about 10 ps.

If the charge carrier is in an electric field $(\vec{E})$, then the total force on the carrier is the sum of the electrical and magnetic forces.

$$\vec{F} = q\vec{E} + q\vec{v} \times \vec{B}$$

When a wire carrying an electric current is placed in a magnetic field, each of the moving charges, which compose the current, experiences the Lorentz force. By combining the Lorentz force law with the definition of electric current, the following equation applies for a straight and stationary wire:

$$\vec{F} = q\vec{E} + I\vec{\ell} \times \vec{B}$$

Where $\vec{\ell}$ is a vector whose magnitude is the length of wire, and whose direction is along the wire, aligned with the direction of conventional current charge flow $I$. Note that the magnetic force does not depend on the sign of the charge carriers creating the current.



- ⊗ B field into the page
- ● red positive carrier
- ● blue negative carrier
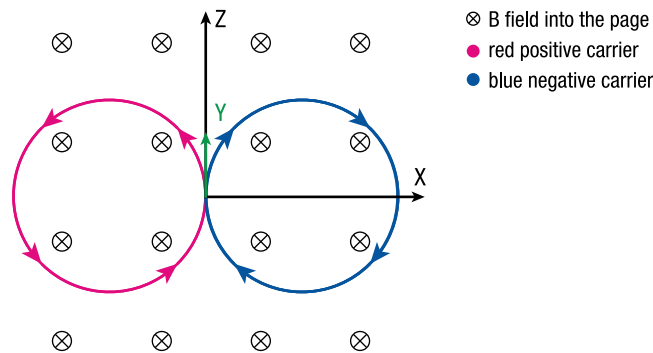
**Figure 9** *The Lorentz force causes the charge carriers to rotate in circles around the field lines.*

A magnetic field exerts a force on particles in the field. The force depends on the velocity of the particle, amount of the charge, and the strength of the field.

## The Hall effect

The fundamental observation of the Hall effect is shown in Figure 10. If a current is flowing in a material in the $x$ direction, and an external magnetic field is applied in the positive $z$ direction, then an electric field is induced in the $y$ direction. This electrical field is proportional to the current and magnetic field. The force on the current by the electric field is balanced by the Lorentz force. The integral of the electrical field across the width of the sample is the Hall voltage. It can be either positive or negative.
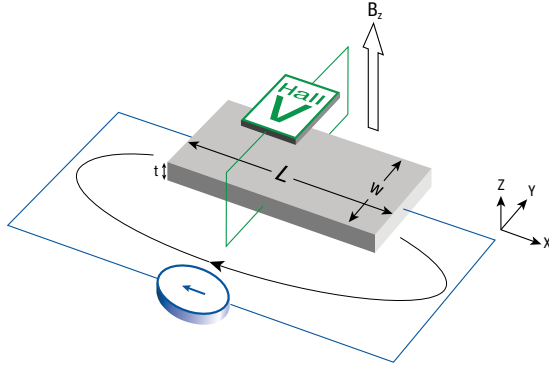


**Figure 10** *Sample showing geometry for the Hall effect.*

In this model the sample is long and thin. The width is $w$ and length $L$. The contacts are such that the current flows only in the positive $x$ direction. The resistance of the sample is $R$. The $x$ component of the electric field is $IR/L$. The $B$ field only has a $z$ component, which is perpendicular to the plane of the sample and the direction of the current flow. The magnetic force is in the $y$ direction and is $-qv_x B_z$. No current can flow out of the sample in the $y$ direction. Carriers in cyclotron orbits (circular orbits that charged particles exhibit in a uniform magnetic field) in the $xy$ plane within the cyclotron radius of $y = 0$ accumulate on the $y = 0$ edge of the sample and deplete on the $y = w$ edge. This generates an electric field in the $y$ direction, $V_{Hall}/w$. When the force from this electric field $(-q\,V_{Hall}/w)$ is equal and opposite to the magnetic force, there is no net force in the $y$ direction, and the current flow is uniform in the $x$ direction. It takes on the order of one half of a cyclotron period (~5 ps) to establish this new steady state.

$$-q\,V_{hall}/w = -qv_x B_z$$

$$v_x = \frac{I}{nqwt}$$

Here $n$ is the carrier density and $t$ is the thickness, hence

$$V_{hall} = \frac{IB_z}{nqt}$$

The Hall coefficient $(R_H)$ is defined as $R_H = \frac{1}{nq}$

In the simplest theory (free electron gas model), the resistivity is related to material properties by $\rho = 1/(nq\mu)$ where $\mu$ is the mobility.

If we measure the resistivity and Hall coefficient, then the following material properties can be derived:

Carrier density: $n = 1/(qR_H)$

Mobility: $\mu = 1/(\rho nq) = |R_H|/\rho$

Carrier type: electrons if $R_H$ is negative; holes if $R_H$ is positive.

**Measurement of Hall voltage in Hall bar samples**

The Hall voltage is typically measured using one of two different geometries: Hall bar or van der Pauw geometry. Figure 11 shows the Hall bar geometry.
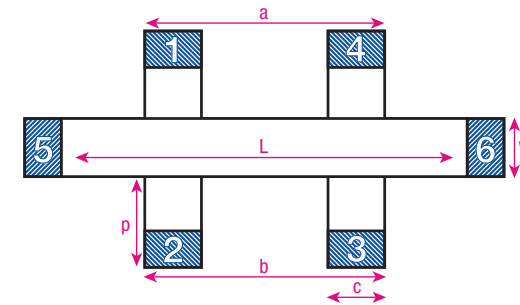


**Figure 11** *A Hall bar; this geometry is often called a 1-2-2-1 Hall bar. Other geometries are possible.*

The Hall voltage is measured with both positive and negative fields.

$$V_{56,34}^{B+} = \frac{V_{34}^{B+}(I_{56}^{+}) - V_{34}^{B+}(I_{56}^{-})}{2}$$

$$V_{56,34}^{B-} = \frac{V_{34}^{B-}(I_{56}^{+}) - V_{34}^{B-}(I_{56}^{-})}{2}$$

$$V_{AHall} = \frac{V_{56,34}^{B+} - V_{56,34}^{B-}}{2}$$

$$V_{56,21}^{B+} = \frac{V_{21}^{B+}(I_{56}^{+}) - V_{21}^{B+}(I_{56}^{-})}{2}$$

$$V_{56,34}^{B-} = \frac{V_{21}^{B-}(I_{56}^{+}) - V_{21}^{B-}(I_{56}^{-})}{2}$$

$$V_{BHall} = \frac{V_{56,21}^{B+} - V_{56,21}^{B-}}{2}$$

$$V_{Hall} = \frac{V_{AHall} + V_{BHall}}{2}$$

This method measures the Hall voltage twice. Ideally, $V_{AHall}$ and $V_{BHall}$ should be the same. Using the two measurements tends to average out any geometric errors.
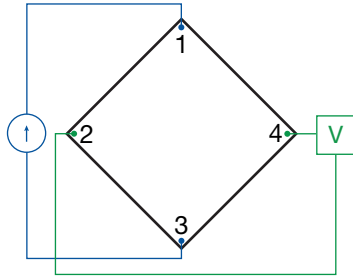
**Figure 12** *Configuration for measuring Hall voltage in a van der Pauw sample.*

The van der Pauw geometry is shown in Figure 12. The current source is connected across the diagonal of the sample and the voltage is measured across the other diagonal.

The voltage is measured at both positive and negative fields, which, as for the Hall bar, eliminates misalignment voltages, as well as positive and negative currents, resulting in four separate measurements. These four measurements are used to calculate the Hall voltage, $V_{Hall}$.

$$V_{13,42}^{B+} = \frac{V_{42}^{B+}(I_{13}^+) - V_{42}^{B+}(I_{13}^-)}{2}$$

$$V_{13,42}^{B-} = \frac{V_{42}^{B-}(I_{13}^+) - V_{42}^{B-}(I_{13}^-)}{2}$$

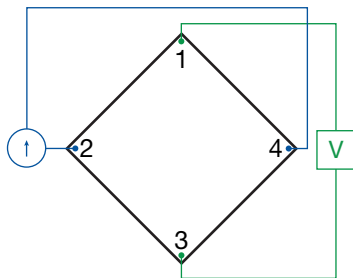$$V_{AHall} = \frac{V_{13,42}^{B+} - V_{13,42}^{B-}}{2}$$



**Figure 13**

$$V_{24,31}^{B+} = \frac{V_{31}^{B+}(I_{24}^+) - V_{31}^{B+}(I_{24}^-)}{2}$$

$$V_{24,31}^{B-} = \frac{V_{31}^{B-}(I_{24}^+) - V_{31}^{B-}(I_{24}^-)}{2}$$

$$V_{BHall} = \frac{V_{24,31}^{B+} - V_{24,31}^{B-}}{2}$$

$$V_{Hall} = \frac{V_{AHall} + V_{BHall}}{2}$$

The principle advantages of measuring van der Pauw samples is that only four contacts are required, sample widths or distances between contacts need not be known, and simple geometries can be used.

A resistivity measurement on a van der Pauw sample takes 8 current settings and voltage measurements, and a Hall voltage measurement on a van der Pauw sample takes 4 current settings and voltage measurements: a total of 12 measurements. A resistivity measurement on a Hall bar sample takes 4 current settings and voltage measurements, and a Hall voltage measurement on a Hall bar sample takes 4 current settings and voltage measurements: a total of 8 measurements.

Disadvantages are that measurements take about twice as long as for Hall bar samples, and errors due to contact size and placement can be significant when using simple geometries.
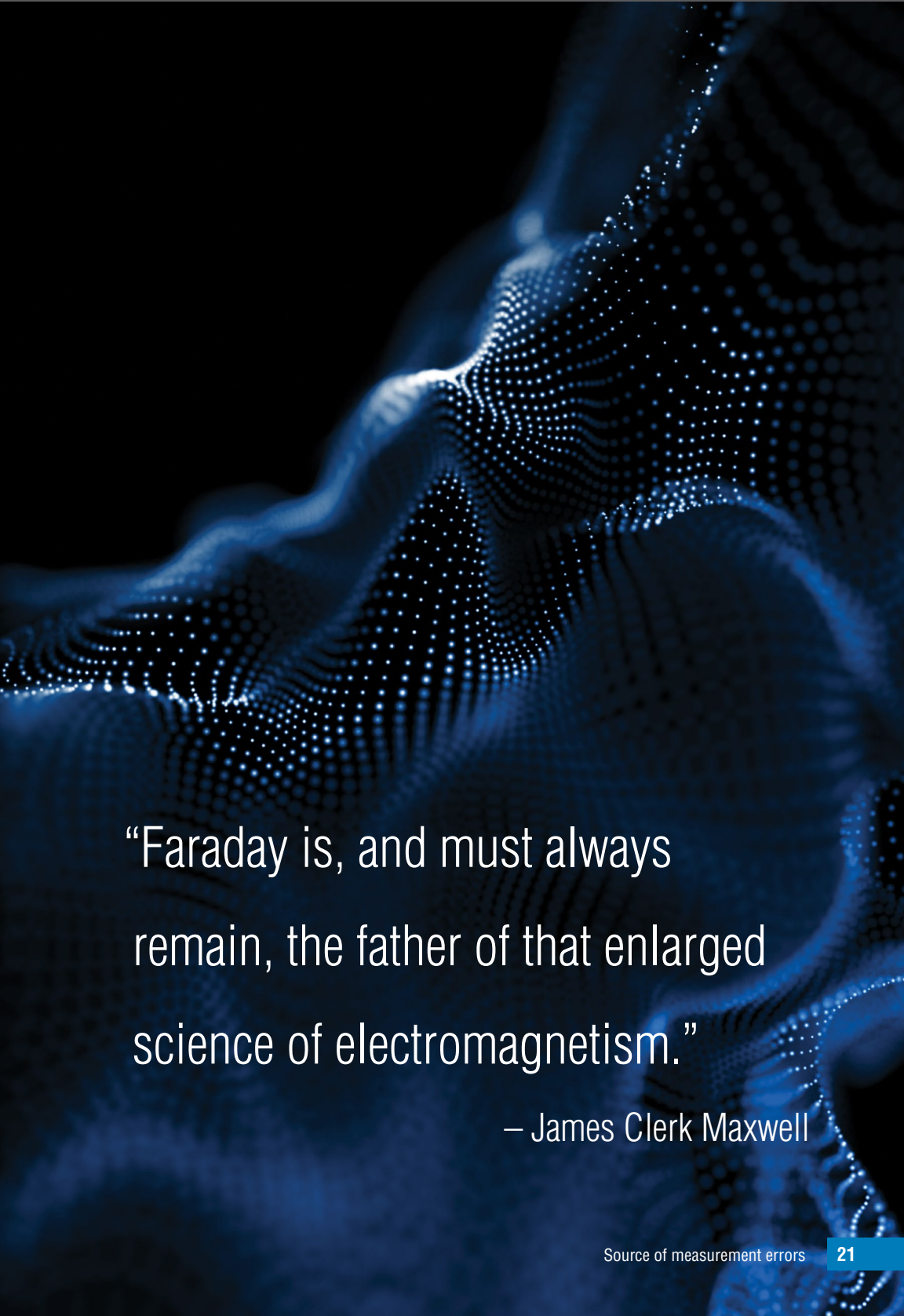
## Source of measurement errors

David C. Look[5] provides an excellent treatment of systematic error sources in Hall effect measurements in the first chapter of his book. There are two kinds of error sources: intrinsic and geometrical.

### Intrinsic error sources

The apparent Hall voltage, $V_{Ha}$, measured with a single reading can include several spurious voltages. These spurious error sources include the following:

1. **Voltmeter offset $(V_o)$:** An improperly zeroed voltmeter adds a voltage $V_o$ to every measurement. The offset does not change with current or magnetic field direction.

2. **Current meter offset $(I_o)$:** An improperly zeroed current meter adds a current $I_o$ to every measurement. The offset does not change with current or magnetic field direction.

3. **Thermoelectric voltages $(V_{TE})$:** A temperature gradient across a sample allows contacts between two different materials (i.e., metallic contacts on a semiconductor) to function as a pair of thermocouple junctions. The resulting thermoelectric voltage is due to the Seebeck effect and is designated $V_{TE}$. Portions of wiring to the sample can also produce thermoelectric voltages in response to temperature gradients. These thermoelectric voltages are not affected by current or magnetic field direction, to first order.

4. **Ettingshausen effect voltage $(V_E)$:** Even if no external transverse temperature gradient exists, the sample can set up its own. The $q\vec{v} \times \vec{B}$ force shunts slow (cool) and fast (hot) electrons to the sides in different numbers and causes an internally generated Seebeck effect. This phenomenon is known as the Ettingshausen effect. Unlike the Seebeck effect, $V_E$ is proportional to both current and magnetic field. This is the one intrinsic error source which cannot be eliminated from a Hall voltage measurement by field or current reversal.

5. **Nernst effect voltage $(V_N)$:** If a longitudinal temperature gradient exists across the sample, then electrons tend to diffuse from the hot end of the sample to the cold end, and this diffusion current is affected by a magnetic field, producing a Hall voltage. The phenomenon is known as the Nernst or Nernst-Ettingshausen effect. The resulting voltage is designated $V_N$ and is proportional to magnetic field, but not to external current.

6. **Righi-Leduc voltage $(V_R)$:** The Nernst (diffusion) electrons also experience an Ettingshausen-type effect since their spread of velocities result in hot and cold sides, and thus again set up a transverse Seebeck voltage, known as the Righi-Leduc voltage, $V_R$. The Righi-Leduc voltage is also proportional to magnetic field, but not to external current.

> "Faraday is, and must always remain, the father of that enlarged science of electromagnetism."
>
> – James Clerk Maxwell

7. **Misalignment voltage** *($V_M$)*: The excitation current flowing through a sample produces a voltage gradient parallel to the current flow. Even in zero magnetic field, a voltage appears between the two contacts used to measure the Hall voltage if they are not electrically opposite each other. If contacts are not identical geometrically and/or not precisely aligned, a misalignment voltage will be produced. Voltage contacts are difficult to align exactly and the misalignment voltage is frequently the largest spurious contribution to the apparent Hall voltage.

The apparent Hall voltage, $V_{Ha}$, measured with a single reading contains all the above spurious voltages:

$$V_{Ha} = V_{Hall} + V_o + V_{TE} + V_E + V_N + V_R + V_M.$$

All but the Hall and Ettingshausen voltages can be eliminated by combining measurements, as shown in Table 1. Measurements taken at a single magnetic field polarity still have the misalignment voltage, frequently the most significant unwanted contribution to the measurement signal. Comparing values of $R_H$ *(+B)* and $R_H$ *(-B)* reveals the significance of the misalignment voltage relative to the signal voltage. A Hall measurement is fundamentally a voltage divided by a current, so excitation current errors are equally as important. Current offsets, $I_o$, are canceled by combining the current measurements, then dividing the combined Hall voltage by the combined excitation current.

| | I | B | V<sub>Hall</sub> | V<sub>M</sub> | V<sub>TE</sub> | V<sub>E</sub> | V<sub>N</sub> | V<sub>R</sub> | V<sub>0</sub> |
|---|---|---|---|---|---|---|---|---|---|
| $V_1$ | + | + | + | + | + | + | + | + | + |
| $V_2$ | − | + | − | − | + | − | + | + | + |
| $(V_1 - V_2)$ | | | $2V_{Hall}$ | $-2V_M$ | 0 | $2V_E$ | 0 | 0 | 0 |
| $V_3$ | + | − | − | + | + | − | − | − | + |
| $V_4$ | − | − | + | − | + | + | − | − | + |
| $(-V_3 + V_4)$ | | | $2V_{Hall}$ | $-2V_M$ | 0 | $2V_E$ | 0 | 0 | 0 |
| $(V_1 - V_2 - V_3 + V_4)$ | | | $4V_{Hall}$ | 0 | 0 | $4V_E$ | 0 | 0 | 0 |

*Table 1* Hall effect measurement voltages showing the elimination of all but the Hall and Ettingshausen voltages by combining readings with different current and magnetic field polarities.

Geometrical error sources in the Hall bar arrangement are caused by deviations of the actual measurement geometry from the ideal of a rectangular solid with constant current density and point-like voltage contacts. The first geometrical consideration with the Hall bar is the tendency of the end contacts to short out the Hall voltage. If the aspect ratio of sample length to width $L/w = 3$, then this error is less than 1%.[6] Therefore, it is important that $L/w \geq 3$. The finite size of the contacts affects both the current density and electric potential in their vicinity and may lead to relatively large errors. The errors are larger for a simple rectangular Hall bar as shown in Figure 14 than for one in which the contacts are placed at the end of arms as shown in Figure 15.
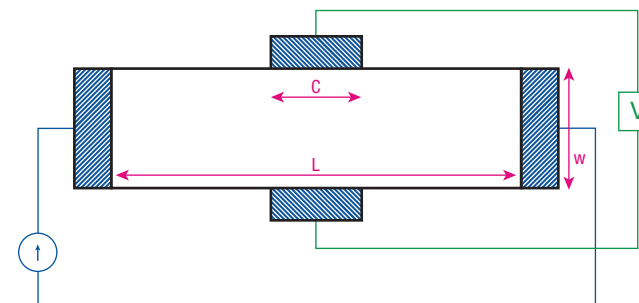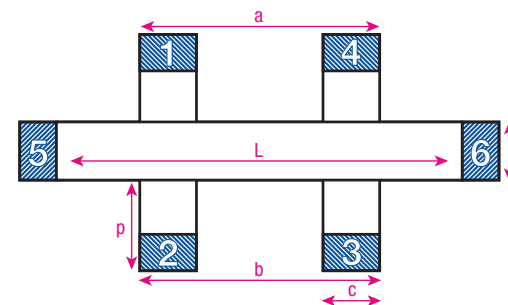


*Figure 14* Hall bar with finite size voltage contacts.

For a simple rectangle, the error in the Hall mobility can be approximated (when $\mu B << 1$) by[7]

$$\frac{\Delta\mu_H}{\mu_H} = 1 - \left[(1 - e^{\frac{-\pi L}{2w}})(1 - \frac{2c}{\pi w})\right]$$

Here, $\Delta\mu_H$ is the amount $\mu_H$ must increase to obtain a true value. If $L/w = 3$, and $c/w = 0.2$, then $\Delta\mu_H/\mu_H = 0.13$ (13%), which is certainly a significant error.



*Figure 15* Hall bar with contact arms.

Placing contacts at the ends of contact arms reduces the contact size error to acceptable levels.[8] The following aspect ratio yields small deviations from the ideal: $p \approx c, c \leq w/3, L \geq 4w.$

Van der Pauw's[4] analysis of resistivity and Hall effect in arbitrary structures assumes point-like electrical connections to the sample. In practice, this can be difficult or impossible to achieve, especially for small samples. The finite-contact size corrections depend on the sample geometry, and, for Hall voltages, the Hall angle $\theta$ (defined by $tan(\theta) = \mu B$, where $\mu$ is the mobility). If $B$ is in tesla, then $\mu$ must be in m²/(V s). If $B$ is in gauss and $\mu$ is in cm²/(V s) then $tan(\theta) = \mu B \times 10^{-8}$. Look[5] presents the results of both theoretical and experimental determinations of the correction factors for some of the most common geometries. We summarize these results here and compare the correction factors for a 1:6 aspect ratio of contact size to sample size.

### Square structures

The resistivity correction factor $\Delta\rho/\rho$ for a square van der Pauw structure as shown in Figure 16 is roughly proportional to $(c/L)^2$ for both square and triangular contacts. At $(c/L) = 1/6$, $\Delta\rho/\rho = 2\%$ for identical square contacts, and $\Delta\rho/\rho < 1\%$ for identical triangular contacts.[9] The Hall voltage measurement error however is much worse. The correction factor $\Delta R_H/R_H$ is proportional to $(c/L)$ and is about 15% for triangular contacts when $(c/L) = 1/6$. The correction factor also increases by about 3% at this aspect ratio as the Hall angle increases from $tan(\theta) = 0.1$ to $tan(\theta) = 0.5$.
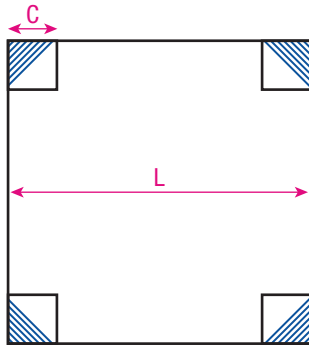
**Figure 16**  Van der Pauw sample with square or triangular contacts.

### Circular structures

Circular van der Pauw structures as illustrated in Figure 17 fare slightly better. Van der Pauw[4] gives a correction factor for circular contacts of

$$\frac{\Delta\rho}{\rho} = -\frac{1}{16\ln 2}\left(\frac{c}{L}\right)^2 \text{ (per contact)}$$

which results in a correction of $\Delta\rho/\rho = -1\%$ for $(c/L) = 1/6$ for four contacts. For the Hall coefficient, van der Pauw gives the correction

$$\frac{\Delta R_H}{R_H} = \frac{2c}{\pi^2 L} \text{ (per contact)}$$

At $(c/L) = 1/6$, this results in a correction of 13% for four contacts.

Van Daal[10] reduced these errors considerably (by a factor of 10 to 20 for resistivity, and 3 to 5 for Hall coefficient) by cutting slots to turn the sample into a cloverleaf, as shown in Figure 18. The cloverleaf structure is mechanically weaker than the square and round samples unless it is patterned as a thin film on a thicker substrate. Another disadvantage is that the "active" area of the cloverleaf is much smaller than the actual sample.
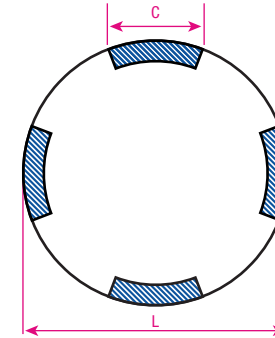
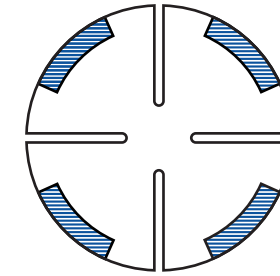**Figure 17**  Circular van der Pauw structure.

**Figure 18**  Cloverleaf van der Pauw sample.

### Greek cross structures

The Greek cross structure shown in Figure 19 is one of the best van der Pauw geometries to minimize finite contact size errors. Its advantage over simpler van der Pauw structures is analogous to placing Hall bar contacts at the ends of arms. David and Beuhler[11] analyzed this structure numerically. They found that the deviation of the actual resistivity $\rho$ from the measured value $\rho_m$ obeyed

$$E = 1 - \frac{\rho}{\rho_m} = (0.59 \pm 0.0006)\, e^{[-(6.23\pm 0.002)\frac{a}{c}]}$$

This is a very small error: for $c/(c + 2a) = 1/6$, where $c + 2a$ corresponds to the total dimension of the contact arm, $E \approx 10^{-7}$. Hall coefficient results are substantially better. De Mey[11,12] has shown that

$$\frac{\mu_H - \mu_{Hm}}{\mu_H} = \frac{\Delta\mu_H}{\mu_H} = 1.045e^{-\pi a/c} \text{ (four contacts)}$$

where $\mu_H$ and $\mu_{Hm}$ are the actual and measured Hall mobilities, respectively. For $c/(c + 2a) = 1/6$, this results in $\Delta\mu_H/\mu_H \approx 0.04\%$, which is quite respectable.
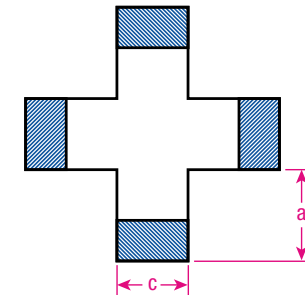
**Figure 19**  Greek cross van der Pauw structure.

## Electrical contacts to semiconducting materials

All direct measurements of the electronic transport properties of a material require adequate electrical contacts between the sample and the measuring instrument. Adequacy depends on the measurement performed. Generally, low resistance "ohmic" contacts are desired. The word "ohmic" ideally means "obeying Ohm's Law," a condition that is technically impossible to achieve in a metal-semiconductor interface.[13] "Ohmic" usually means a contact with a small resistance compared to the resistance of the sample being studied, and therefore insignificant non-linear current-voltage characteristics.

Several parameters describe electrical contacts to semiconductors. The quantity of greatest interest is the contact resistivity or specific contact resistance, denoted by $\rho_c$ and usually measured in $\Omega \cdot cm^2$. Contact resistivity is the product of the contact resistance $\rho_c$ and the area $A$ of the contact. Other common contact parameters include the barrier height $\Phi_B$, measured in eV (electron volts), and the semiconductor doping concentration, measured in $cm^{-3}$.

Three primary mechanisms govern current transport across a metal-to-semiconductor interface: thermionic emission, field emission, and thermionic-field emission.[14] They differ mainly by the interface potential barrier height and width as determined by the work function of the metal, the semiconductor electron affinity, and the semiconductor doping concentration near the interface.

Thermionic emission is important when both the barrier and doping concentration are low. In thermionic emission, electrons thermally excited to energies above the barrier pass directly over it. As a result, contact resistance where thermionic emission dominates depends strongly on temperature.

Field emission is important when both the barrier and doping concentration are high. A high doping concentration reduces the width of the carrier depletion region near the semiconductor's surface. This in turn produces a thin barrier that electrons tunnel through directly. A field emission is only weakly dependent on temperature.

Thermionic-field emission is important when both barrier and doping concentration are moderate. In thermionic-field emission, electrons are thermally excited part way up the potential barrier, at which point they tunnel the rest of the way through. Thermionic-field emission is moderately temperature-dependent. Typically, some sort of thermionic-field emission is the most likely transport mechanism.

There are several methods of contact deposition: applying metal-bearing paints and pastes, melting metals directly on the semiconductor surface, evaporation, sputtering, molecular beam epitaxy, ion-implantation, and others. Once deposited on the semiconductor, the contact may be thermally annealed by conventional oven, laser or electron beam, or rapid thermal annealing/processing (RTA or RTP), in which halogen lamps rapidly heat the semiconductor to the annealing temperature and hold it there for a short time (typically 10 to 30 s).

Whichever deposition technique is used, placing adequate electrical contacts on a semiconductor sample requires attention to detail and good technique in order to minimize non-ohmic effects. Four important considerations for ensuring the quality of sample contacts include choice of connection technique, contact material, contact construction, and stability of the connection.

1. **Connection method:** A contact can either be a metal pad with a wire bonded to the pad or a metal pad with a probe needle as illustrated in Figure 20. The choice of connection method will depend on both the type of sample that will be tested and accessibility in the test fixture. Pads with bond wires are more suitable for a sample housed in a cryogenic chamber for low temperature measurements. Some samples or situations may preclude the use of contacts layered on the material; in those cases, probe needle contact methods may be required.

2. **Contact material:** High conductivity materials should be used for metal pads. The details of the pad construction depend on the material. For instance, for p-type silicon, the preferred contacts are aluminum. For gallium oxide ($Ga_2O_3$) the preferred material is titanium/gold (Ti/Au) or titanium/aluminum (Ti/Al) stacks. Options for attaching wires to the contacts include conductive paint, indium solder, or silver epoxy. The choice depends on how well the material adheres to the sample.

3. **Contact construction:** Ensure that metal pads are in the appropriate locations as defined by the van der Pauw or Hall bar structures. Also make sure pad size is small so that the ratio between the contact width $w$ and the length $L$ of the sample structure exceeds 1:10.

4. **Stability of the connection:** Bonded wires lack flexibility but produce constant forces on the sample. Probe contacts can have variable pressure on the sample, particularly in variable temperature measurements (due to thermal expansion and contraction), and be prone to sources of vibration. These effects can vary contact. Ensuring that each probe applies the same pressure to the sample eliminates a variable in contact resistance among the multiple probes.
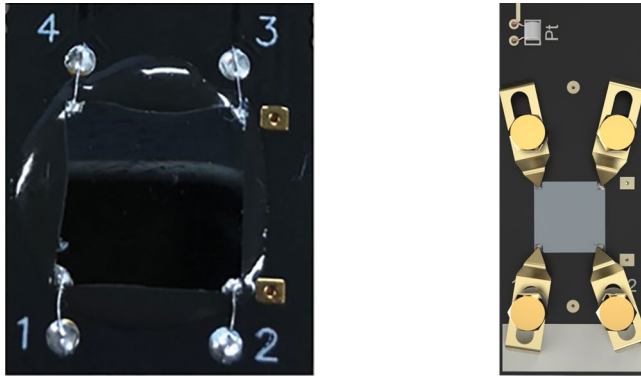
*Figure 20* *Square van der Pauw structure showing wire bonding connections to an InAs sample (left) and probe connections to a bare sample card (right).*

The ohmic quality of the contacts can be analyzed by making current-voltage *(I-V)* measurements of contact pairs. The more linear the *I-V* curves, the more ohmic the contacts are. By measuring the *I-V* curves and correlating the curve to an ideal linear function using a regression fit method, the ohmic quality of the contact can be assessed. Using a correlation coefficient of greater than 0.9999 is recommended. The non-linear nature of the contacts can be minimized by using a source current that effectively operates in the linear region of the diode-like contact. Determining a source current that results in a correlation coefficient greater than 0.9999 is an iterative, trial-and-error process. A source current that results in a high linear correlation for the contact-pairs is the recommended magnitude to be used for resistivity and Hall measurements.

### Voltage vs. current

V = 416.3290E3 * I + 44.29977E-3, correlation = 941.8816E-3
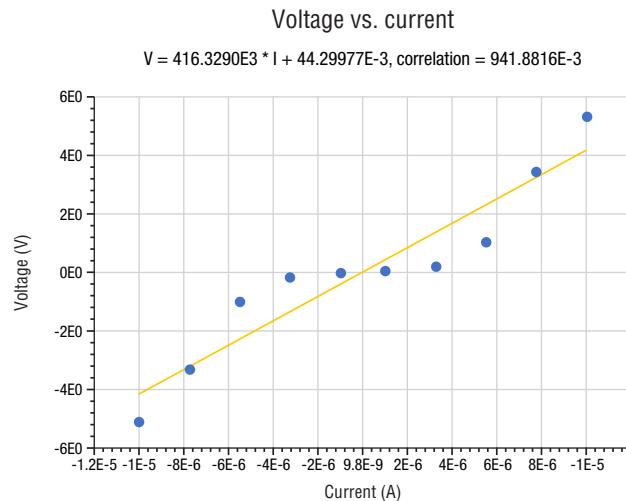


*Figure 21* *A non-ohmic contact showing diode-like behavior. The equation is the best fit straight line.*

### InAs contact check   R² = 1
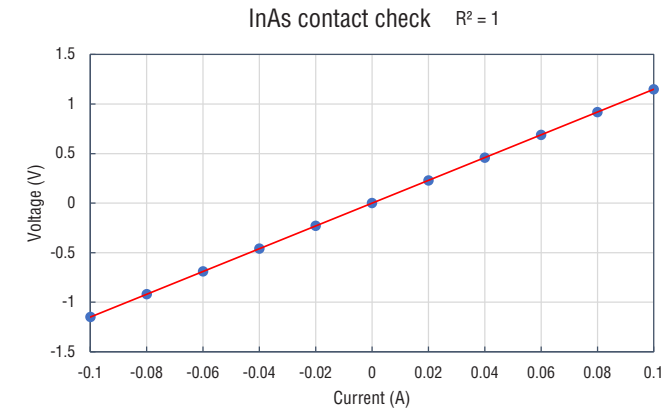


*Figure 22* *A very good ohmic contact. This is the I-V curve for the InAs sample on the left in Figure 20.*

Testing to ensure the quality of ohmic contacts to the test sample is a critical step in gaining confidence in the quality of the resultant Hall measurements. If ohmic connections are highly resistive, which can be the case with certain materials such as gallium nitride (GaN) and gallium oxide (GaO), then Hall effect measurements can provide results that include the properties of the contacts along with the properties of the material under test. Figure 21 shows an *I-V* curve with diode-like behavior. The correlation coefficient of the fit is 0.94. Figure 22 is the *I-V* curve of an indium arsenide (InAs) sample shown on the left in Figure 20. The *I-V* curve is a straight line with a correlation coefficient of 1.0.

There can be other reasons for non-linear behavior of *I-V* curves. If the material changes temperature, for example from self-heating, during the measurement of the *I-V* curve, then the resistance of the sample will change during the measurement. Since the resistance of the sample is reflected in the slope of the *I-V* curve, the slope will change at each point and the curve will be non-linear. Figure 23 is the *I-V* curve for a p-type silicon (Si) sample with indium contacts. The correlation coefficient is 0.99, and the non-linearity is due to self-heating of the Si sample. Often the self-heating can be reduced by decreasing the current. Decreasing the current by a factor of 10 will decrease the power dissipated in the sample by a factor of 100, assuming the resistance of the sample has not changed.

**Contact measurement with self heating**
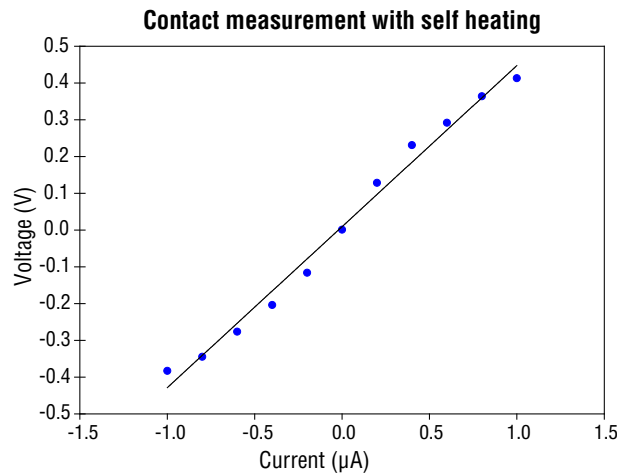


**Figure 23** *I-V curve of a p-type Si sample with indium contacts. The correlation coefficient is 0.99 and the I-V curve shows the effect of self-heating.*

|  | Recommended contact material | Contact resistance |
|---|---|---|
| Si p-type | Al-Si alloy | 15 $\Omega$ $\mu m^2$ |
| Si n-type | Al-Si alloy | 90 $\Omega$ $\mu m^2$ |
| SiC | Ti | 0.0092 $\Omega$ $cm^2$ |
| $Ga_2O_3$ | Ti/Au | 0.0002 $\Omega$ $cm^2$ |
| n-GaAs | AuGe/Ni | |
| p-GaAs | Au/Pd | |
| n-InP | Au/Ti | |

**Table 2** *Some recommended contact materials for various semiconductor samples.*

The recommended contact materials for various semiconductor materials tabulated in Table 2 are only intended to be general guidelines. Care should be exercised — requirements and methods may change for smaller samples and devices because they will require smaller contact dimensions. In addition, the method can change due to other factors like surface preparation and surface defects. Furthermore, a reduction in temperature of a sample can change an ohmic contact into a non-ohmic contact. During a variable temperature measurement, the contact quality should be checked at every measurement temperature. If good ohmic contacts cannot be obtained at room temperature, heating the sample may allow a measurement, but could possibly change the sample material properties.

Finally, if the lateral dimensions of the sample are scaled down equally, the resistance of the sample will remain the same and the current requirements also remain the same. The current density in a small device will increase. In this situation, the contact must have lower specific contact resistance to be usable.

## Methods of Hall measurements

The Hall effect is a well-known method to determine the carrier concentration, carrier type, and when coupled with a resistivity measurement, the mobility of a material. The traditional method used in Hall measurements uses a DC magnetic field. This method has a long history of successful measurements on a wide range of materials including semiconductors.[5] However, materials with low mobility, such as those important in solar cell technology, thermoelectric technology, and organic electronics, are very difficult to measure using DC measurement techniques. In this section we will re-introduce a long-neglected method using AC fields.[15,16] Although mentioned in the literature for many years, this technique had little advantage for measuring materials for which the DC measurement provides good results (i.e., high mobility materials).

### Review of DC field Hall measurement protocol

There is a very well-developed methodology for measuring the Hall effect and resistivity using DC fields.[5] The methodology is designed to remove the unwanted effects from the measured voltage. The following sections provide a brief summary of this methodology. These explanations are based on the definitions provided here.

The Hall voltage is proportional to the magnetic field $(B)$, current $(I)$, and Hall coefficient $(R_H)$ and depends inversely on the thickness $(t)$. In an ideal geometry the measured Hall voltage is zero with zero applied field. However, the voltage measured in a practical experiment $(V_{measured})$ also includes a misalignment voltage $(V_m)$ and a thermoelectric voltage $(V_{TE})$. The misalignment voltage is proportional to the resistivity of the material $(\rho)$, the current, and a factor $(\alpha)$ that depends on the geometry. This factor converts resistivity of the material to resistance between the two Hall voltage contacts. The thermoelectric voltage arises from contacts between two different materials and is independent of the current. The thermoelectric voltage does depend on any thermal gradients present in the sample. The measured Hall voltage is:

$$V_{measured} = \frac{R_H I B}{t} + V_m + V_{TE}$$

$$V_{measured} = \frac{R_H I B}{t} + \alpha \frac{\rho}{t} I + V_{TE}$$

The mobility $(\mu)$ is the Hall coefficient divided by the resistivity. Since the Hall coefficient $(R_H)$ is equal to the mobility $(\mu)$ times the resistivity $(\rho)$, $V_{measured}$ can be given by:

$$V_{measured} = \frac{\rho I}{t}(\mu B + \alpha) + V_{TE}$$

The factor $\alpha$ can be as small as zero (for no offset), but typically it is about 1.

### Using current reversal to remove the effects of the thermoelectric voltage

Current reversal can be used to remove the unwanted effects of thermoelectric voltage $(V_{TE})$. As explained in the first section, thermoelectric voltage does not depend on current or field direction; current reversal exploits this characteristic to remove the effects of $V_{TE}$.

### Using field reversal to remove the effects of the misalignment voltage

Field reversal, as explained in the first section, can be used to remove the unwanted effects of the misalignment voltage. The Hall voltage depends on the magnetic field, but the misalignment voltage does not. As with the thermoelectric voltage, measurement of the voltage at positive and negative fields is used to remove the misalignment voltage.

### Disadvantages of the DC method

For low mobility materials, the quantity $\mu B$ can be very small compared to $\alpha$. When the expression $(V_{measured}(B_1) - V_{measured}(B_2))$ is calculated, the subtraction between the two large numbers gives a small result. Any noise in the measurement can easily dominate the actual quantity, and consequently, produce imprecise results. This is often the reason that Hall measurements on low mobility materials give inconsistent carrier signs.

A second problem is that the two measurements $V_{measured}(B_1)$ and $V_{measured}(B_2)$ can be separated in time by a significant amount. The time to reverse the field of a magnet can vary from seconds to minutes depending on the magnet configuration. The misalignment voltage $V_m = \rho I \alpha / t$ depends on the resistivity of the material. If the material changes temperature between the two measurements $V_{measured}(B_1)$ and $V_{measured}(B_2)$, the misalignment voltage will change, and the subtraction will not completely cancel the misalignment voltage. The un-canceled misalignment voltage will be included in the calculation of the Hall coefficient.

### What is the misalignment voltage and how to control it?

The misalignment voltage $V_m$, the measured voltage in a Hall measurement at zero field, is often the largest intrinsic error in a Hall measurement. It is a purely geometric effect. If the sample was a perfect square and the contacts were mathematical point contacts on the corner of the sample, the misalignment voltage would be zero. Any deviation from this ideal will result in non-zero misalignment voltage.

**Perfect square point contacts B = 0**
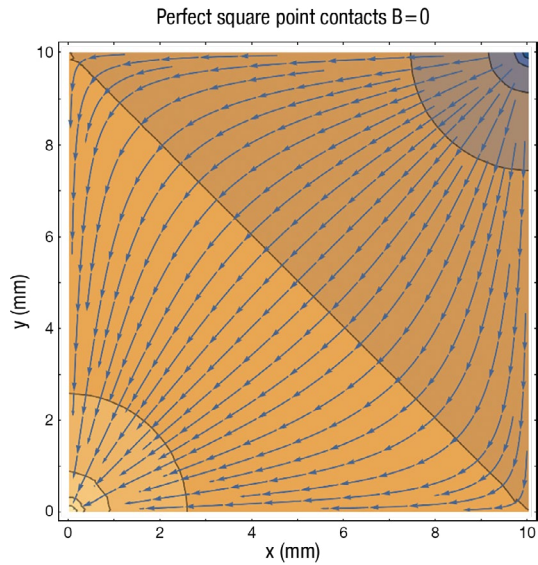
***Figure 24*** *Equipotential lines and current flow for a square sample with point contacts.*

Figure 24 shows the equipotential lines and current flow for a perfect square sample with point contacts. The misalignment voltage in this case is 0. The modeled sample has a sheet resistivity of 1000 Ω/sqr and a mobility of 1 cm²/(V s). The measurement current is 1 mA, and the Hall voltage for this sample at $B = 1\ T$ is 100 µV.



**$V_{13,42}$ B = 0 square finite pads**
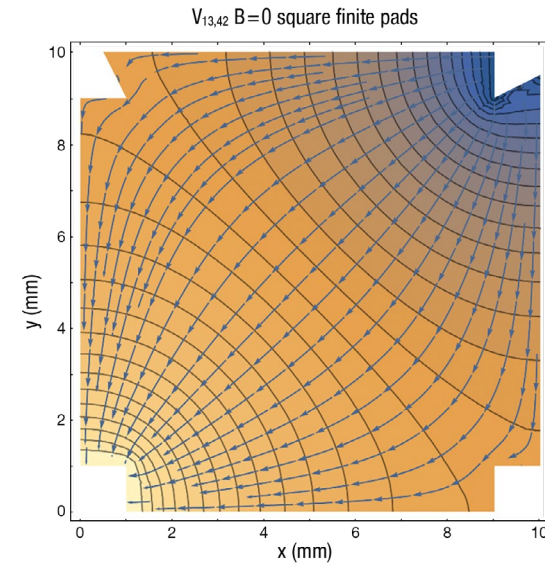
***Figure 25*** *Perfect square; deformed pads.*

Figure 25 shows the same sample but with finite deformed contact size. In this case the misalignment voltage is 66 mV for the same excitation.



**$V_{13,42}$ B = 0 rectangle finite pads**
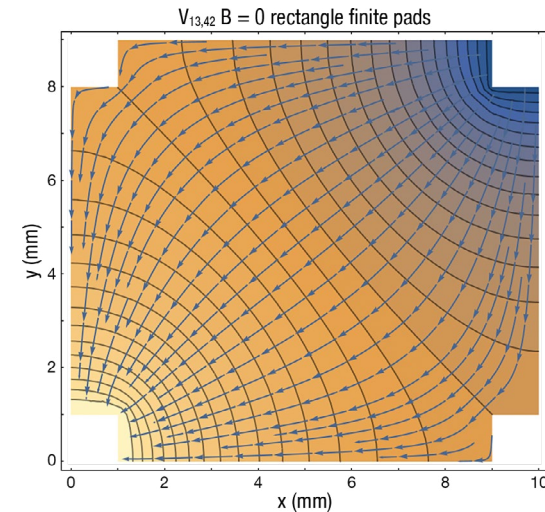
***Figure 26*** *Rectangle sample (width/length = 0.9) with 4 symmetric finite contacts. The misalignment voltage is 127 mV.*

Finally, Figure 26 shows the same sample but with a length to width ratio of 0.9, with finite contact size. In this case the misalignment voltage is 127 mV.

Examples of variable temperature and variable magnetic field DC field Hall measurements for various materials are presented later in this guide.

## AC field Hall measurements

A second method to remove the effect of the misalignment is to use an AC magnetic field. If the magnetic field is a sinusoidal signal $(B(t) = B\sin(\omega t))$, then in the quasi-static approximation, the Hall voltage will become time dependent as well, $V_H(t) = (I\rho\mu/t)\,B\sin(\omega t)$. The misalignment voltage is independent of the magnetic field, and consequently remains a DC voltage. The measured voltage is now

$$V_{measured}(B) = \frac{\rho I}{t}\left(\mu B\sin(\omega t) + \alpha\right)$$

Using a lock-in amplifier (LIA) in the measurement electronics can separate the desired AC signal from the undesired DC signal with a high degree of precision. Removing the DC signal, we are left with

$$V_{measured}(B) = R_H\, IB_{RMS}\sin(\omega t)$$

However, there is a new term in the measured voltage that is proportional to the time derivative of the magnetic field, and to the inductance of the sample and the leads used in the measurement. If the proportionality constant is $\beta$, the measured voltage is written as:

$$V_m(B) = R_H\, IB_{RMS}\sin(\omega t) - \beta\omega B_{RMS}\cos(\omega t)$$

If the LIA is perfectly phased to the magnetic field, the x and y channels will read

$$V_x = R_H\, IB_{RMS}$$
$$V_y = -\beta\omega B_{RMS}$$

If there is a phase error of $\varphi$ then the x and y channels will read

$$V_x = R_H\, IB_{RMS}\cos(\varphi) + \beta\omega B_{RMS}\sin(\varphi)$$
$$V_y = R_H\, IB_{RMS}\sin(\varphi) - \beta\omega B_{RMS}\cos(\varphi)$$

Since this is an AC signal, the LIA will measure this term as well as the Hall voltage term. Since this term is independent of the current, just like the thermoelectric voltage, one method is to use current reversal to remove this term, after which the x and y channels will read

$$V_x = R_H\, IB_{RMS}\cos(\varphi)$$
$$V_y = R_H\, IB_{RMS}\sin(\varphi)$$

The Hall voltage is then

$$V_{Hall} = R_H\, IB_{RMS} = \sqrt{V_x^2 + V_y^2}$$

## The effect of thermal drifts

The major disadvantage of AC field measurements is that, since the inductance of typical electromagnets is large, the frequency of the AC field will be small. Typically, the frequency is on the order of 0.1 Hz to 0.2 Hz. The measurement time for a single Hall voltage measurement can take as much as an hour or longer. During this time the temperature of the sample can change. This change of temperature can be driven by changes in the environment of the sample or self-heating of the sample by the current used for the measurement. In either case this change in temperature will change the resistivity of the sample, typically on the order of 1% per degree change in temperature. This change in resistivity will change the misalignment voltage during the measurement. Hence the misalignment voltage is no longer a DC voltage but a complex AC voltage with frequency components at the same frequency of the AC magnetic field frequency. Hence there will be a voltage measured by the LIA that is due to the thermal drift. This is in addition to the voltage measured by the LIA due to the Hall voltage.

Figure 27 is an AC field measurement of a zinc oxide (ZnO) sample. The oscillations in the plot are the Hall voltage. The amplitude of the AC magnetic field was 1 T. The Hall voltage (peak to peak) is about 1.5 mV. The misalignment voltage, at the start of the measurement, is approximately -698.5 mV. The measurement time was 1000 s. At the end of the measurement the misalignment voltage is approximately -701.0 mV. The change in the misalignment voltage is 2.5 mV, which is approximately the same as the Hall voltage.
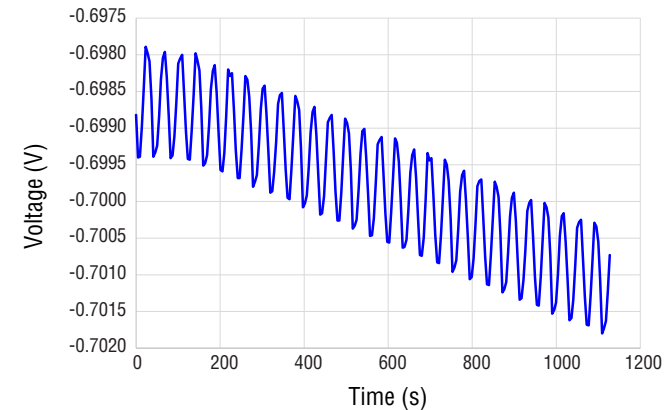


**Figure 27** *Variation in Hall voltage over time due to temperature variation in a sample. The oscillations are the measured voltage in a low frequency AC field. The amplitude of the oscillation is the Hall voltage. The offset is the misalignment voltage. The misalignment voltage is about 450 times larger than the Hall voltage.*

The effects of self-heating can also have a major impact on AC field Hall measurements. One generally assumes that by increasing the current used in a measurement, the Hall voltage will increase, which in turn will increase the signal to noise ratio (SNR). However, as is shown in Figure 28 this is not always the case. In this measurement for a bismuth vanadium oxide ($BiVO_2$) sample the excitation current was increased from 1 to 4 mA, and yet the SNR actually decreased from approximately 3 to 0.5.

It should be noted that while AC field Hall measurements can be made using conventional electromagnets, it is not possible to sinusoidally vary the field in high field superconducting magnets for AC field Hall on a practical time scale owing to their very large inductance.

Examples of AC field Hall measurements for various materials are presented later in this guide.

SNR vs. current AC field
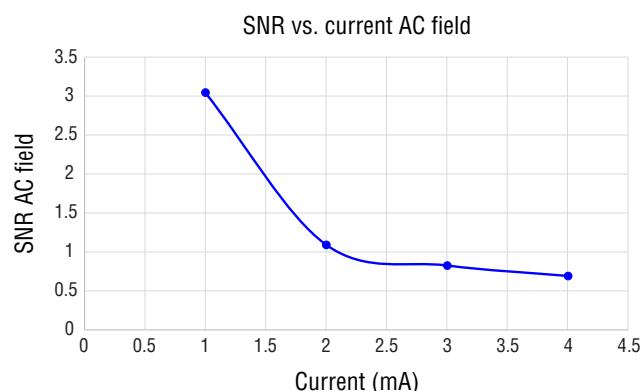
Figure 28  *The signal-to-noise ratio (SNR) of the $BiVO_2$ sample decreases with increasing current. This results from the current self-heating the sample and the misalignment voltage slowly changing during the measurement.*

Contributors to reciprocity theory

**1853 — Hermann von Helmholtz[17]**
**1883 — Leon Thevenin[18]**
Both men independently deduced the theorem known as the Helmholtz-Thevenin theorem that a linear network with current sources, voltage sources, and resistors can be represented by an equivalent voltage source and equivalent series resistance. (https://en.wikipedia.org/wiki/Thévenin%27s_theorem)

**1896 — Hendrik Lorentz**
Devised the theorem, now known as the Lorentz reciprocity theorem, that a voltage source and a current source in a network can be interchanged without affecting the network.

**1926 — Hans Mayer[19] Edward Norton[20]**
Both men independently derived the Mayer-Norton Theorem, which indicates that a linear network can be represented by an equivalent current source and parallel resistance.

**1931 — Lars Onsager[21]**
Derived the Onsager Reciprocal Relations, which defined the equality of ratios between flows and forces in thermodynamic systems.

**1987 — H. H. Sample, W. J. Bruno, S.B. Sample, and E. K. Sichel[22]**
Developed a static electromagnetic reciprocity principle involving reversal of a magnetic field when a reciprocal measurement is made.

**2017 — Jeffrey Lindemuth[23]**
Patented a technique, at Lake Shore Cryotronics, using reciprocity and current spinning to make accurate Hall measurements in a minimum amount of time without reversing the polarity of the magnetic field.

### Review of reciprocity theorems
Every electrical engineering student is, at some point, probably taught the reciprocity theorem for electrical networks. Simply stated, the theorem says that for a linear passive network with current source and voltmeters, the measured voltage is the same if the current source and voltmeter are interchanged (Figure 29).[24]
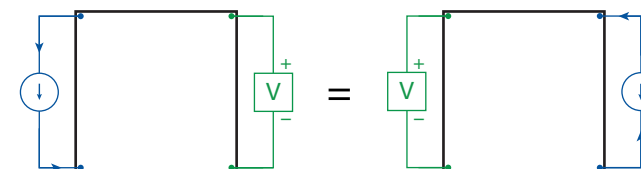
Figure 29  *In this example the voltage reading for the same current input is the same in both diagrams.*

### The reverse field reciprocity theorem

The above theorem applies for no external magnetic field. The theorem can be extended to include the case where there is an external magnetic field.[22] If there is an external field *(B)*, then the reciprocity theorem states that if the voltage measurement and current source are interchanged, then the equality holds only if the magnetic field polarity is switched (Figure 30).
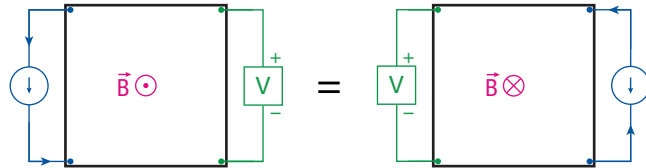


*Figure 30  The reverse field reciprocity theorem. If there is an external magnetic field, then in addition to interchanging the current source and voltmeter, the external field must be reversed. The only restriction on the network (sample) is that it is linear (in current and voltage) and passive.*

We can use this theorem to eliminate the physical field reversal from the Hall measurement. The effective field reversal time can be much less than the time required to reverse the field in an electromagnet, and considerably less time than it takes to reverse the field in a superconducting magnet. The reversal only involves changing the connections to the sample, which can be performed at moderate (millisecond) time scales. This quick field reversal translates into fast measurement times, overcoming one of the disadvantages of the AC field method. The sample, during the measurement, only sees a DC magnetic field, so the Hall voltage measured is at *B* or *-B*. In the AC field method, the sample sees a sinusoidally changing field and if the Hall voltage of the sample is not linear, in addition to the fundamental Hall voltage, harmonics will be generated.

### Spinning current methods

Spinning current is a method used by the Hall sensor community to remove misalignment voltages from a Hall sensor when it is not possible to use field reversal.[25,26,27,28] The technique is based on the field reciprocity theorem and is intended for the high mobility materials typically used in Hall sensors.
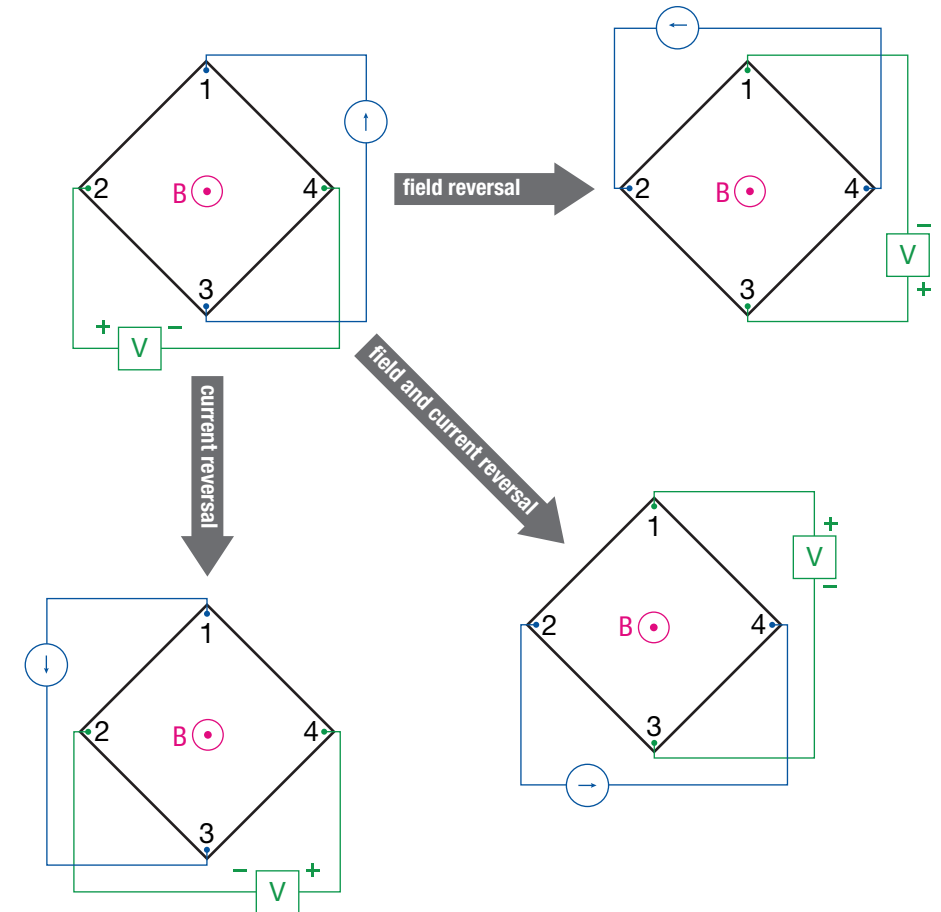


*Figure 31  The spinning current method. The field is effectively reversed by interchanging the voltage and current leads. A Hall voltage is obtained by a sequence of 4 measurements.*

In the spinning current method illustrated in Figure 31, the four measurements can be made rapidly by, for instance, solid state switching. The time sequence of these four measurements is:

$$(1)\ V_{m1} = I\frac{R_H B}{t} + I\frac{\alpha\rho}{t} + V_{TE1}$$

$$(2)\ V_{m2} = -I\frac{R_H B}{t} + I\frac{\alpha\rho}{t} + V_{TE2}$$

$$(3)\ V_{m3} = -I\frac{R_H B}{t} - I\frac{\alpha\rho}{t} + V_{TE1}$$

$$(4)\ V_{m4} = I\frac{R_H B}{t} - I\frac{\alpha\rho}{t} + V_{TE2}$$

From these four measurements, the Hall voltage can be calculated as $(V_{m1}-V_{m2}-V_{m3}+V_{m4})/4$.

### The FastHall™ method[23]

The spinning current method works well for high mobility materials, but for low mobility materials it suffers from the same issues as DC field Hall. The subtractions in the equation for the Hall voltage will subtract two large voltages to extract a small voltage difference, in the case of low mobility materials. The FastHall™ method extends the spinning current methods to optimize the measurement of low mobility materials as well as high resistance materials.

The FastHall™ method uses the advantage of the high-speed measurement coupled with control of both the current and field sequence to optimize the Hall measurement (Figure 32).
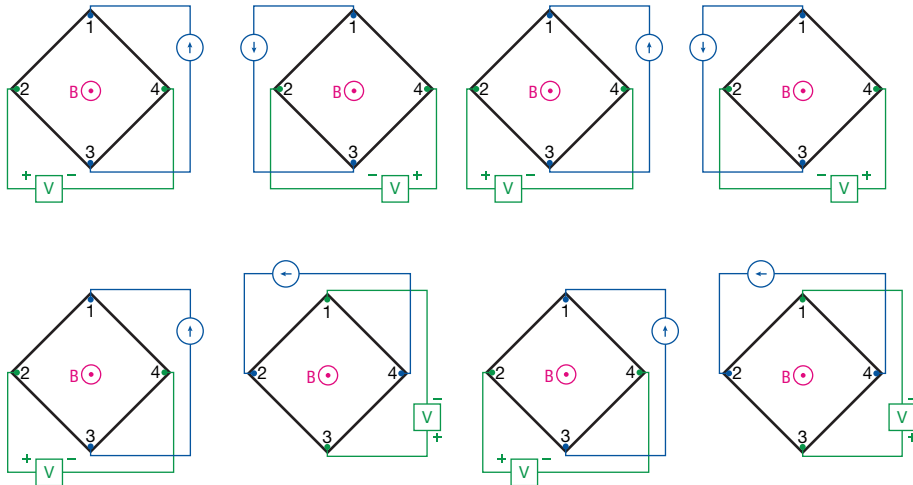
**Figure 32** *The upper row is a sequence of current reversal, at fixed field which can be thought of as an AC current measurement. The bottom row is a sequence of field reversals, at a fixed current which can be thought of as an AC field measurement.*

### Comparison of FastHall™ and DC field Hall

Table 3 shows a comparison of samples measured with DC field Hall and the FastHall™ method. The samples are indium gallium zinc oxide (IGZO) and zinc oxide (ZnO). The mobility of these samples is relatively low. There is good agreement between the DC field Hall method and the FastHall method. The FastHall method is up to 100 times faster, for the same standard error in the measurement.

| Sample | | Conventional DC field Hall | | | M91 FastHall™ | | |
|---|---|---|---|---|---|---|---|
| $V_M$ | Mobility cm²/(V s) | Hall voltage | Standard error | Time (s) | Hall voltage | Standard error | Time (s) |
| IGZO | 4.20E-03 | 9.11 | -0.00105 | 3.00E-07 | 114 | -0.00105 | 5.10E-07 | 1.26 |
| IGZO | 2.00E-04 | 12.50 | -9.40E-05 | 1.00E-06 | 114 | -9.50E-05 | 2.84E-07 | 32.8 |
| ZnO | 1.60E-05 | 4.76 | -8.60E-06 | 3.00E-08 | 114 | -8.77E-06 | 6.62E-07 | 6.76 |

**Table 3** *Comparison of DC field Hall and FastHall™*

### Comparison of AC field Hall and FastHall™

Table 4 is a comparison of two low mobility materials. AC field must be used for the measurement because of the low mobility. The first sample is polycrystalline silicon (poly-Si) with a sheet resistivity of 15.6 Ω/sqr and a mobility of 2.5 cm²/V s. The second is titanium oxide (TiO) with a moderately high sheet resistivity of 133 kΩ/sqr and a mobility of 0.01 cm²/V s. There is excellent agreement between the AC field method and the FastHall method for both samples.

| | Resistivity (Ω/sqr) | | Mobility cm²/(V s) | |
|---|---|---|---|---|
| | AC field Hall | M91 FastHall™ | AC field Hall | M91 FastHall™ |
| Poly-Si | 15.72 | 15.67 | 2.42 | 2.57 |
| TiO | 133,000 | 137,000 | 0.011 | 0.0102 |

**Table 4** *Comparison of AC field Hall and FastHall™. In all cases the approximate measurement times were approximately 3600 s for the AC field Hall, and 15 s for the FastHall.*

### Comparison of FastHall™ and DC field Hall with a gate bias

Figure 33 shows the Hall voltage vs. gate bias for a graphene sample. The data were taken with a Lake Shore Cryotronics probe station with a 2.5 T vertical field superconducting magnet and the Model 8425 Hall measurement system. The DC field data are the red dashed line, and the FastHall data are the blue solid line. The DC field method required field reversal at each point. The FastHall method did not require field reversal. The measurement time per point is 510 s for the DC method and 115 s for the FastHall method, a 4.5 times reduction in measurement time.

It should be noted that the FastHall technique is only applicable to van der Pauw samples, and that Hall bar samples cannot be measured using the technique. The reverse field reciprocity theorem applies to 2D current flows. In a Hall bar sample, the current flow is 1D.
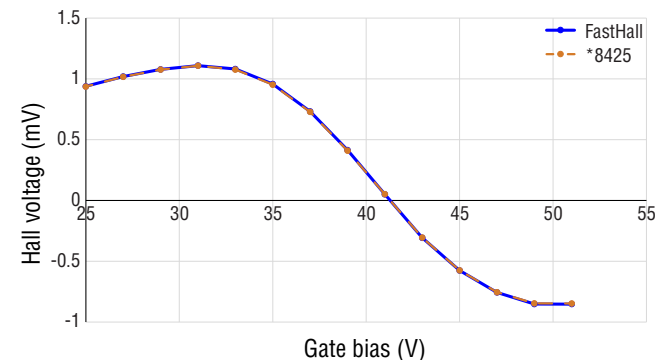
Sample courtesy of Richard Kiehl, Arizona State University.

**Figure 33** *Hall voltage vs. gate bias for a graphene sample*

# Advanced Hall measurements

## Thin films

Many materials tested using Hall effect measurements are thin films. Thin film samples are grown on substrates, which can be conductive and can create additional paths for the source current. To avoid the scenario of a substrate effectively creating a parallel resistive shunt current path that results in increased source current, an insulating substrate or a substrate which is very lightly doped compared with the thin film should be used. Another method to increase substrate resistivity is to apply a voltage to the substrate with a polarity that reduces the carrier density in the substrate. If either of these options are not possible, then the substrate should be characterized, independently, with Hall and resistivity measurements, which then can be used as a correction factor for the measurements on the thin film sample.

## Gate bias measurements

For some materials, adding a control voltage, or a gate bias voltage, via additional contacts added to the sample provides information on material behavior in the presence of a bias voltage. When a voltage is applied on the gate contact, the carrier density and the carrier mobility through the material are altered. The polarity of the gate bias voltage can either increase or decrease the carrier density and carrier mobility. The use of a gate bias helps to assess how well the material can be used as a transistor-like device.

## Photoexcited measurements

Many semiconductor materials are sensitive to light energy. Photoexcited measurements are often used on these materials. Photoexcitation increases carrier density as well as carrier mobility. Using photoexcitation, the properties of a material as a function of light intensity and light wavelength can be characterized. The Hall effect measurements are conducted with a test setup in which a controlled light source is directed onto the sample. When photoexcitation is not being studied, then test samples should be shielded from light sources to remove the variability in carrier density and carrier mobility caused by light energy. Care should be taken to make sure Hall measurements are collected in a light tight environment to keep from impacting the results with stray light.

## The Hall factor

Earlier we defined the mobility by the equation $\vec{v} = \mu\vec{E}$. The velocity of a carrier is proportional to the electric field. This is called the drift mobility and labeled as $\mu D$. The Hall mobility, $\mu_{Hall}$, or simply $\mu$ is related to the drift mobility by

$$\frac{\mu_{Hall}}{\mu_D} = r$$

The Hall factor $r$ is a function of temperature and magnetic field, [29,3] and is always greater than 1. The Hall coefficient is then $R_H = r/nq$. In the limit of high field, $r \to 1$, and we recover the previous result $R_H = 1/nq$. The Hall factor $r$ is usually close to one and it is often assumed that $r = 1$. This will introduce an error of <30% for most materials.[3]

## Intrinsic semiconductors

An intrinsic semiconductor — an undoped semiconductor at a finite temperature — will always have both electron and hole carriers. The electron density is $n$, and the hole density is $p$. The mobility of the electrons is $\mu_n$ and the mobility of the holes is $\mu_p$. The expression for the Hall coefficient of an intrinsic semiconductor is[3]

$$R_H = \frac{r(p - b^2 n)}{q(p + bn)^2}$$

$$b = \frac{\mu_n}{\mu_p}$$

We can recover the previous results for extrinsic materials. For instance, for $p$ doped material $(p \gg n)$ $R_H = r/(qp)$.

## Variable temperature DC field Hall measurements

The Hall effect measurement provides the carrier concentration, mobility, and carrier type of a semiconductor. All three of these parameters are temperature dependent. Measurements of the Hall effect as a function of temperature yields a wealth of useful information about the electronic transport mechanisms in a semiconductor, the doping in and impact of defects on the material, etc. Following are several examples.

### Low-compensated GaAs

The first example is the electrical properties of low-compensated gallium arsenide (GaAs).[30] In this work, two samples of GaAs were characterized with Hall effect over a temperature range of 5 K to 380 K. The data were fit to two models to determine the donor concentration $(N_D)$ and acceptor concentration $(N_A)$. In addition, one of the fitting models also determines the activation energy $(E_{D0})$ and the degeneracy factor $(C)$.

The first model fits the carrier density $n(T)$. The model used is based on a charge balance equation[31]

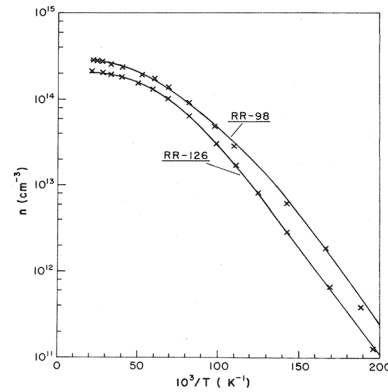$$n + N_A = \frac{N_D}{1 + n/\varphi}$$

$$\varphi = \frac{2(2\pi m_n^* k)^{3/2}}{h^3} CT^{3/2} e^{-E_{D0}/kT}$$

$$Eq.\,4$$

Figure 34 is a plot of the carrier density and fits to equation 4 for both samples.

**Figure 34** *Data and fit of variable temperature carrier concentration.*

The second method was fitting the mobility $\mu(T)$ to the Boltzmann equation. A variety of scattering terms were included in the fits. Refer to reference 30 for details of the fit. Figure 35 is a plot of the mobility data and fits.
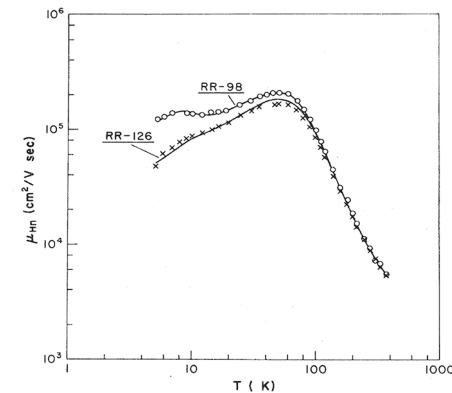
**Figure 35** *Mobility data and fit to Boltzmann equation for two GaAs samples.*

## Magnetoresistance of bismuth (Bi) film

The second example is a variable temperature measurement of a Bi film.[32] The resistance and magnetoresistance (MR) were measured at different temperatures as shown in Figure 36. In addition, the Hall coefficient was measured from 80 K to 300 K. The MR results indicated a large linear MR from compensation of the two carriers in Bi.
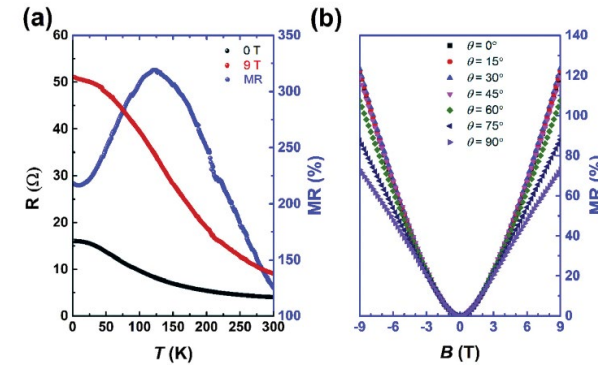
**Figure 36** *Resistance and MR of Bi film.*

Temperature dependent measurements of the Hall coefficient shown in Figure 37 indicate that Bi is p-type at room temperature, but the Hall coefficient changes sign to n-type at approximately 120 K. The change of carrier type is driven by an increasing contribution of surface states as temperature decreases. The temperature at which the Hall coefficient changes sign is approximately the same temperature of the maximum MR, indicating the role of compensation in the MR effect in Bi.
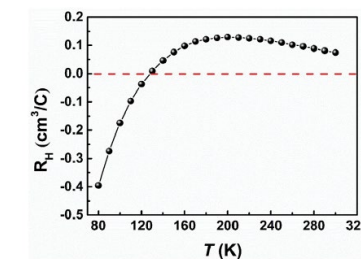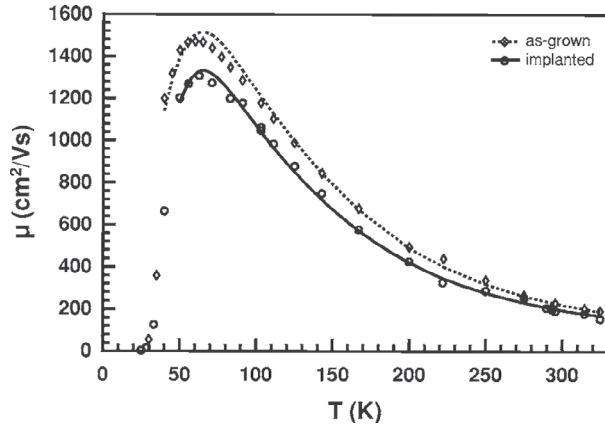
**Figure 37** *Temperature dependence of Hall coefficient for a Bi film.*

## Defects in zinc oxide (ZnO)

The third, and final, example used variable temperature Hall measurements of ZnO to determine defect levels.[33] In addition to Hall measurements, deep level transient spectroscopy (DLTS) measurements were performed. DLTS is a method to determine the activation energy of traps in semiconductors. The conclusion from analysis of the Hall data in Figure 38 and Figure 39 is that the dominant donor has an activation energy of 51 meV. In addition, there are more shallow donors that influence the carrier concentration below 70 K. There are also negatively charged intrinsic defects, probably due to oxygen vacancies. These conclusions were also supported by DLTS measurements.

***Figure 38*** *Hall mobility vs temperature of ZnO samples.*
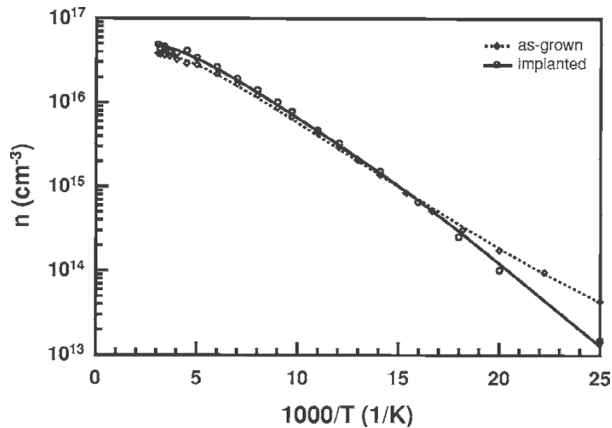
***Figure 39*** *Carrier concentration vs temperature for ZnO samples.*

## Single carrier conductivity in a magnetic field

We have been writing Ohm's law as $E = \rho J$, and we have been assuming that the resistivity $\rho$ is a scalar quantity. This means that the electric field and the current are parallel. When we start to study the Hall effect this assumption is not valid. We have seen that a current in the $x$ direction, in the presence of a magnetic field in the $z$ direction will generate an electric field in the $y$ direction. There is also an electric field in the $x$ direction due to the current in the $x$ direction.

To handle this case, the resistivity must become a tensor. A tensor is a more general "proportionality" constant between two vectors. It is usual to represent a tensor as a matrix. For instance, for a 2D problem, we would write Ohm's law as a vector equation:

$$\begin{pmatrix} E_x \\ E_y \end{pmatrix} = \begin{pmatrix} \rho_{xx} & \rho_{xy} \\ \rho_{yx} & \rho_{yy} \end{pmatrix} \begin{pmatrix} J_x \\ J_y \end{pmatrix}$$

From very general thermodynamics arguments developed by Onsager,[21] it is possible to derive these relations among the elements of the resistivity tensor:

$$\rho_{xx} = \rho_{yy}$$
$$\rho_{xy} = -\rho_{yx}$$

The diagonal element of the resistivity tensor is the same as the scalar resistivity present with no magnetic field. The off diagonal terms are just the Hall resistance, which in the 2D case is $BR_H$. This gives a simple result for the resistivity tensor for 2D Hall effect:

$$\begin{pmatrix} \rho & -BR_H \\ BR_H & \rho \end{pmatrix}$$

The conductivity is also a tensor. The conductivity is still the inverse of the resistivity. To get the conductivity tensor, we need to find the matrix inversion of the resistivity matrix:

$$\sigma = \frac{1}{\rho^2 + B^2 R_H^2} \begin{pmatrix} \rho & BR_H \\ -BR_H & \rho \end{pmatrix}$$

This is the conductivity tensor in terms of parameters measured in a Hall measurement $(\rho$ and $R_H)$. Using the relations between $\rho$ and $R_H$ and carrier density $(n)$ and mobility $(\mu)$ we can also write the conductivity tensor as:

$$\sigma = \begin{pmatrix} \dfrac{nq\mu}{1 + (\mu B)^2} & \dfrac{nq\mu^2 B}{1 + (\mu B)^2} \\ -\dfrac{nq\mu^2 B}{1 + (\mu B)^2} & \dfrac{nq\mu}{1 + (\mu B)^2} \end{pmatrix} = \begin{pmatrix} \sigma_{xx}(B) & \sigma_{xy}(B) \\ -\sigma_{xy}(B) & \sigma_{xx}(B) \end{pmatrix}$$

**Variable field DC field Hall measurements**

Of course, these two representations of the conductivity tensor are equivalent:

$$\sigma_{xx}(B) = \frac{nq\mu}{1 + (\mu B)^2} = \frac{\rho}{\rho^2 + B^2 R_H^2}$$

$$\sigma_{xy}(B) = \frac{nq\mu^2 B}{1 + (\mu B)^2} = \frac{BR_H}{\rho^2 + B^2 R_H^2}$$

For a single carrier, even though $\rho$ and $R_H$ are independent of field, the conductivity will show field dependency. Figure 40 shows $\sigma_{xx}(B)$ and $\sigma_{xy}(B)$ for a single carrier with mobility 5 m$^2$/(V s) and density $1 \times 10^{22}$ m$^{-3}$, for fields to 1 T.
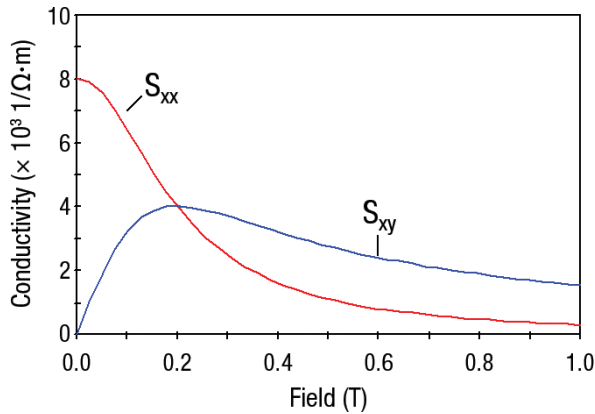


**Figure 40** $\sigma_{xx}(B)$ and $\sigma_{xy}(B)$ for a single carrier with mobility 5 m$^2$/(V s) and density $1 \times 10^{22}$ m$^{-3}$, for fields to 1 T.

Some useful properties[34] of $\sigma_{xx}$ and $\sigma_{xy}$:

- $\sigma_{xy}(0) = 0$

- $\sigma_{xy}(B)$ is an extremum at $\mu B = 1$

- $\sigma_{xy}(\infty) = 0$ and approaches $0$ as $1/B$

- $\sigma_{xy}(-B) = -\sigma_{xy}(B)$

- $\sigma_{xx}$ has an inflection point at $\mu B = 1$

- $\sigma_{xx}(\infty) = 0$ and approaches $0$ as $1/B^2$

- $\sigma_{xx}(B) > 0$ for all finite $B$

- $\sigma_{xx}(-B) = \sigma_{xx}(B)$

**Multicarrier analysis**

Up to this point we have assumed that the conductivity of every elemental charged carrier in the material is the same. For most semiconducting materials this is not the case. Multiple carriers can arise from several conditions: parallel conduction in unique layers, changing material parameters due to strain in the layers, intrinsic carriers, and multi-valley conduction in bulk semiconductors, etc.

When a second through N$^{th}$ carrier are present in a material, it is assumed that each carrier acts independently and the conductivity of the carriers add (the carriers conduct in parallel just like parallel resistors):

$$\sigma_{xx}(B) = \sum_j^N \frac{n_j q_j \mu_j}{1 + \mu_j^2 B^2} \quad Eq.\,1$$

$$\sigma_{xx}(B) = \frac{\rho(B)}{\rho^2(B) + (BR_H(B))^2} \quad Eq.\,2$$

$$\sigma_{xy}(B) = \sum_j^N \frac{n_j q_j \mu_j^2 B}{1 + \mu_j^2 B^2} \quad Eq.\,3$$

$$\sigma_{xy}(B) = \frac{BR_H(B)}{\rho^2(B) + (BR_H(B))^2} \quad Eq.\,4$$

$$\rho(B) = \frac{\sigma_{xx}}{(\sigma_{xx}^2 + \sigma_{xy}^2)}$$

$$R_H(B) = \frac{\sigma_{xy}}{B(\sigma_{xx}^2 + \sigma_{xy}^2)}$$

**Measurement procedure**

Measure the resistivity, $\rho_{xx}(B)$ and Hall coefficient, $R_H(B)$, at various magnetic fields using full Hall measurement protocol (DC field) with field reversal and current reversal. At each field $(B_k)$ convert the measured resistivity and measured Hall coefficient to experimental conductivity, $\sigma_{xx}exp(B_k)$ and $\sigma_{xy}exp(B_k)$ using equation 2 and equation 4. Fit the experimental conductivity to the model in equation 1 and equation 3.

A variety of methods have been used to fit measured data to the model. We will briefly review of few of these methods.

## Nonlinear least squares fit

The classic method of fitting experimental data to a theory is using least squares. The model used here is nonlinear in the fitting parameters, so some form of nonlinear least squares fitting must be used. If the number of carriers is 2 (for instance an electron and a hole) there are analytical methods[35] that can be used, but these methods are not easily extended to more than 2 carriers.

The $\chi^2$ function to minimize is:[36]

$$\chi^2 = \sum_{k=1}^{M} \left( \left( \sigma_{xx}^{exp}(B_k) - \sum_{j}^{N} \frac{n_j q_j \mu_j}{1 + \mu_j^2 B_k^2} \right)^2 + \left( \sigma_{xy}^{exp}(B_k) - \sum_{j}^{N} \frac{n_j q_j \mu_j^2 B_k}{1 + \mu_j^2 B_k^2} \right)^2 \right)$$

Here $M$ is the number of magnetic fields, and $N$ is the number of carriers in the model. There are $3N$ parameters in the fit. They are the carrier density, sign, and mobility of the carrier for each carrier. This can be cut to $2N$ parameters if the fit of the equations is rewritten in terms of the zero-field resistivity $\rho_{0j} = n_j q_j \mu_j$ and a signed mobility $\mu_j$. $\mu_j$ is positive for holes and negative for electrons. Then the $\chi 2$ function is:

$$\chi^2 = \sum_{k=1}^{M} \left( \left( \sigma_{xx}^{exp}(B_k) - \sum_{j}^{N} \frac{\rho_{0j}}{1 + \mu_j^2 B_k^2} \right)^2 + \left( \sigma_{xy}^{exp}(B_k) - \sum_{j}^{N} \frac{\rho_{0j} \mu_j B_k}{1 + \mu_j^2 B_k^2} \right)^2 \right)$$

Yu-Ming Lin et al.[37] have successfully used this method to analyze epitaxial multi-layer graphene. They determined the number of carriers to be 3 by comparing the quality of the fit to the experimental data.

## Mobility spectrum analysis

One of the disadvantages of the non-linear least squares method is that the number of carriers *(N)* is not a fit parameter. It must be determined by some other method. Beck and Anderson[38] proposed replacing the discrete sum of the number of carriers to a weighted integral of conductivity density functions (CDF).

$$\sigma_{xx}(B) = \int_{-\infty}^{\infty} \frac{s^p(\mu) + s^n(\mu)}{1 + \mu^2 B^2} d\mu$$

$$\sigma_{xy}(B) = \int_{-\infty}^{\infty} \frac{(s^p(\mu) - s^n(\mu))\mu B}{1 + \mu^2 B^2} d\mu$$

Here $s^p(\mu)$ is the CDF for holes and $s^n(\mu)$ is the CDF for electrons and $\mu$ is the mobility. Although Beck and Anderson were not able to solve these integral equations, they did derive some limits on the CDF. Their work sparked a variety of approximations to the solutions. S. Kiatgamolchai et al.[39] developed solutions based on a maximum entropy method and D. Chrastina et al.[40] used Bryan's[41] algorithm to find solutions. A collaboration between the Naval Research Lab and University of Western Australia developed qualitative mobility spectrum analysis (QMSA)[42,43] for solving these integral equations.

An example of QMSA measurements on an indium phosphide (InP) pseudomorphic high electron mobility transistor (pHEMT) structure[44] is shown in Figure 41 and Figure 42. Figure 41 shows the measured resistivity and Hall coefficient at different magnetic fields up to 8 T recorded in a Lake Shore Cryotronics Model 9709 9 T superconducting magnet-based Hall system. Figure 42 shows the QMSA spectrum derived from the data. It shows two electron carriers. One carrier has a mobility of 11,700 cm$^2$/(V s) and is identified as the 2-dimensional electron gas (2DEG) carrier in the channel layer of the pHEMT. The other carrier has a mobility of 596 cm$^2$/(V s) and is identified as the carrier in the cap layer of the pHEMT device.
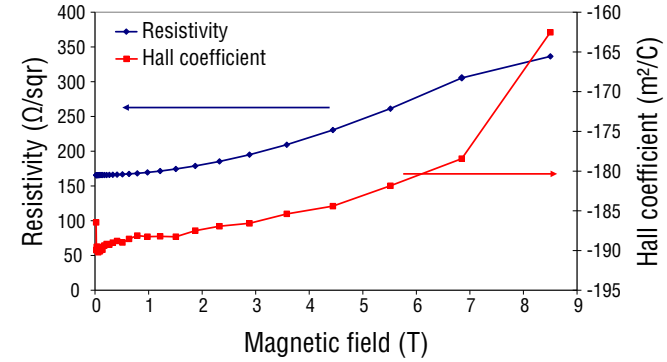


**Figure 41** *Resistivity and Hall coefficient vs. magnetic field for an InP pHEMT structure.*
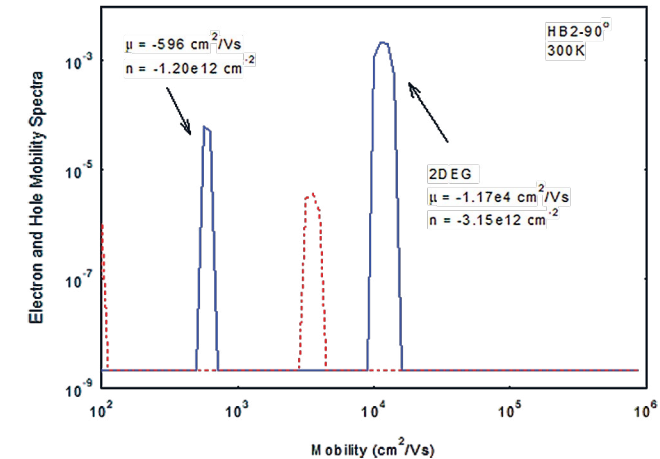


**Figure 42** *QMSA spectrum derived from the data in Figure 41. The spectrum shows two electrons. The red dotted peak is an artifact of the fitting algorithm.*

An example of parallel conduction in a bulk material, gallium antimony (GaSb) is shown in Figure 43. Antimonide compounds, like GaSb, are used for optical applications. In GaSb the energy difference between the $\Gamma$ band and $L$ band is typically less than 0.1 eV.[45] Reported ranges are between 0.075 and 0.090 eV. Hence, for temperatures above about 150 K both bands are occupied and contribute to the conduction in GaSb. Band theory calculations confirm that the $\Gamma$ band electron mobility is higher than the $L$ band electron mobility.[46] This is an example of a bulk material that requires variable field Hall and QMSA to understand the transport properties of the material. Figure 43 shows the QMSA spectrum of GaSb. At 300 K the $L$ band electron has a mobility of 464 cm$^2$/(V s), and the $\Gamma$ band electron has a mobility of 4127 cm$^2$/(V s).
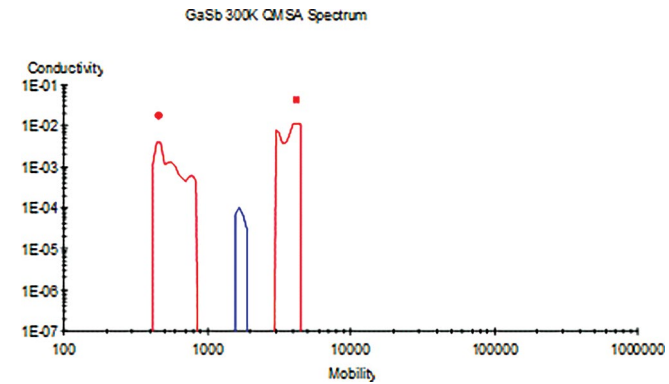


**Figure 43** *QMSA spectrum of GaSb showing two band conduction. The blue peak is an artifact of the fitting algorithm.*

*Variable temperature and variable field*

Using multi-carrier analysis at different temperatures, the mobility of each carrier in a multi-carrier system can be extracted as a function of temperature.[47] Each mobility mechanism (phonon scattering, impurity scattering, etc.) has a different temperature dependency. In Figure 44, the blue dots are the mobility of a carrier extracted from variable field Hall data by QMSA. The temperature-dependent mobility is fit to a combination of the various scattering mechanisms shown in the plot. The scattering mechanisms are combined using Matthiessen's rule. The orange line is the fit to the data.
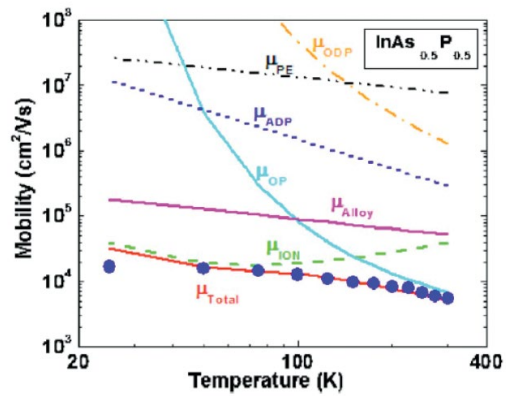
**Figure 44**  *Mobility vs. temperature for InAsP sample.*

## Hall-effect analysis on transition-metal-dichalcogenides (TMD)[48]

Eight natural and synthetic TMD crystals were measured using both DC and AC field Hall methods. Both p-type and n-type materials were included in this study. There was good agreement between the AC and DC methods on all eight samples. The results are tabulated in Table 5.

| Sample (ID) | B field type | Carrier type | Hall mobility cm²/(V s) | Resistivity (Ω·cm) | Carrier concentration (cm⁻³) |
|---|---|---|---|---|---|
| MoS$_2$ (S1) | DC | P | 4.571 | 18.66 | $7.318 \times 10^{16}$ |
| | AC | P | 4.442 | 18.37 | $7.647 \times 10^{16}$ |
| MoS$_2$ (S2) | DC | P | 171.3 | 0.30 | $1.056 \times 10^{17}$ |
| | AC | P | 170.9 | 0.30 | $1.059 \times 10^{17}$ |
| Nb-MoS$_2$ (S3a) | DC | P | 6.204 | 0.014 | $7.427 \times 10^{19}$ |
| | AC | P | 6.189 | 0.014 | $7.445 \times 10^{19}$ |
| Nb-MoS$_2$ (S3b) | DC | P | 7.962 | 0.019 | $4.068 \times 10^{19}$ |
| | AC | P | 7.551 | 0.019 | $4.296 \times 10^{19}$ |
| MoS$_2$ (S4) | DC | N | 124.8 | 10.71 | $4.666 \times 10^{15}$ |
| | AC | N | 113.9 | 10.69 | $5.127 \times 10^{15}$ |
| MoSe$_2$ (S5) | DC | N | 103.1 | 11.67 | $5.187 \times 10^{15}$ |
| | AC | N | 105.6 | 11.72 | $5.045 \times 10^{15}$ |
| MoTe$_2$ (S6) | DC | N | 61.10 | 0.359 | $2.844 \times 10^{17}$ |
| | AC | N | 62.09 | 0.351 | $2.866 \times 10^{17}$ |
| WSe$_2$ (S7) | DC | N | 142.8 | 9.576 | $4.565 \times 10^{15}$ |
| | AC | N | 130.5 | 9.672 | $4.944 \times 10^{15}$ |
| HfSe$_2$ (S8) | DC | N | 7.767 | 0.18 | $4.471 \times 10^{18}$ |
| | AC | N | 7.422 | 0.18 | $4.680 \times 10^{18}$ |

**Table 5** Comparison of AC and DC field Hall measurements for eight TMD samples.

## N-type iron pyrite (FeS$_2$) thin films[49]

Iron pyrite was made in an ampoule with different sulfurization pressures. AC field Hall measurements were performed on all the synthesized pyrite films. The results shown in Figure 45 consistently indicate that all films are n-type with very low mobility values ranging from 1.74 to $6.22 \times 10^{-3}$ cm²/(V s).
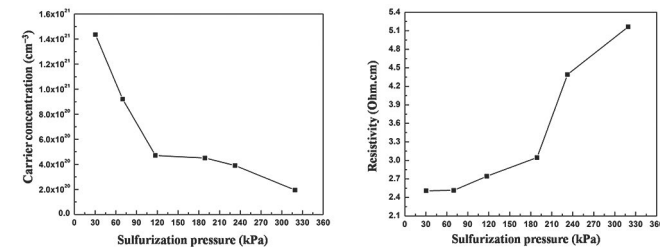
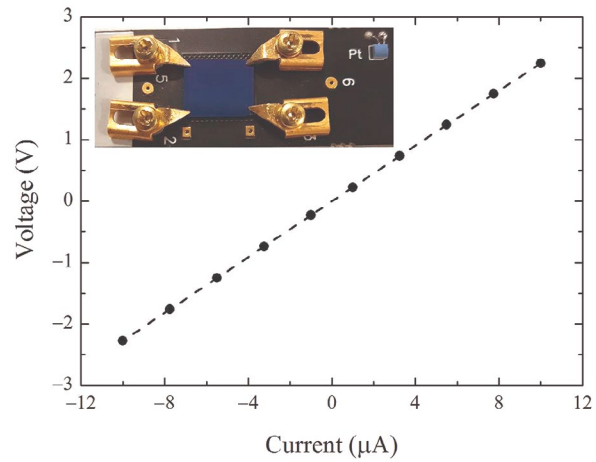**Figure 45** Hall measurement of iron pyrite at different sulfurization pressures.

On the left in Figure 45 the majority charge carrier concentration decreases by an order of magnitude for an order of magnitude increase in the sulfurization pressure. The sulfur to iron ratio increased with pressure; the corresponding drop in the sulfur vacancy concentration is expected, and since sulfur vacancies act as donors, the observed drop in the charge carrier concentration is expected. It in turn has contributed towards the increase in the resistivity as shown in the right of Figure 45.

## Wide spectral photo response of layered platinum diselenide (PtSe$_2$) based photodiodes[50]

Vertical hybrid Schottky barrier diodes (SBDs) of 2D PtSe$_2$ thin films were fabricated on crystalline n-type silicon. The diodes were fabricated by transferring large-scale layered PtSe$_2$ films. The PtSe$_2$ films were characterized with AC field Hall measurements. The 2-point linear $I$-$V$ measurement of the PtSe$_2$ sample with starting platinum thickness of 1 nm is shown in Figure 46, indicating good ohmic contacts. Note that for all resistance and Hall measurements of the sample, the 2-point ohmic correlation factor is accurate to at least 0.99995, and the solution to the 4-point van der Pauw equation gives an $F$ value of 0.99. A photograph of the sample mounted on the Hall measurement card is shown in the inset of Figure 46, and a summary of the Hall results are tabulated in Table 6.

**Figure 46**  *I-V curve for PtS$_2$ sample.*

| Number of PtSe$_2$ layers | 5 to 6 |
|---|---|
| % of measurement accuracy | 100% |
| Carrier type | p-type |
| Mobility (cm$^2$/V s) | 3.5 |
| Carrier concentration (cm$^{-3}$) | $1.89 \times 10^{20}$ |
| Resistivity (Ω·cm) | $9.53 \times 10^{-3}$ |

**Table 6** *Summary of Hall measurements for PtS$_2$ sample.*

This book has focused entirely on the ordinary Hall effect and mostly the ordinary Hall effect in semiconductors. However, there are a variety of other measurements that include the term "Hall effect." Some of these are quite new while others, like the anomalous Hall effect (AHE) in magnetic materials, have been known and studied for many years.

## Spin Hall effect (SHE) and inverse spin Hall effect (ISHE)

The SHE is a transport phenomenon consisting of the appearance of spin accumulation on the lateral surfaces of a sample carrying electric current. The opposing surface boundaries will have spins of opposite sign. It is analogous to the classical Hall effect, where charges of opposite sign appear on the opposing lateral surfaces in an electric-current carrying sample in a magnetic field. In the case of the classical Hall effect, the charge buildup at the boundaries is in compensation for the Lorentz force acting on the charge carriers in the sample due to the magnetic field. No magnetic field is needed for the SHE, which is a purely spin-based phenomenon. The SHE belongs to the same family as the anomalous Hall effect, which also originates from spin-orbit interactions.[51]
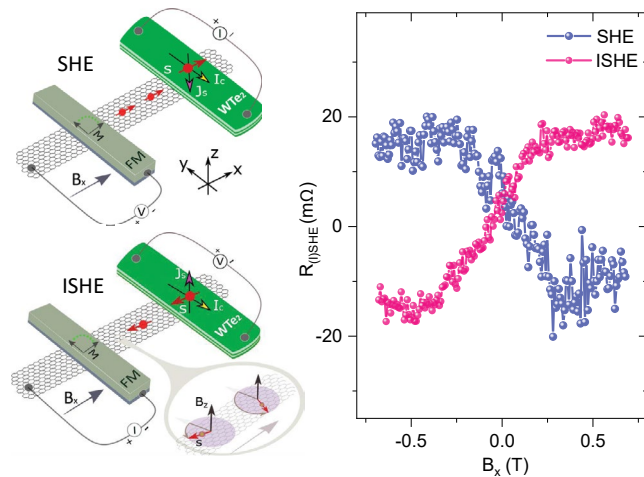
**Figure 47** *On the left are schematic diagrams of SHE and ISHE measurement configurations; on the right is the change in SHE and ISHE resistance.*

In ferromagnetic materials (and paramagnetic materials in a magnetic field), the Hall resistivity includes an additional contribution, known as the anomalous Hall effect (AHE) or the extraordinary Hall effect (EHE), which depends directly on the magnetization of the material, and is often much larger than the ordinary Hall effect. Note that this effect is not due to the contribution of the magnetization to the total magnetic field. For example, in nickel, the anomalous Hall coefficient is about 100 times larger than the ordinary Hall coefficient near the Curie temperature, but the two are similar at very low temperatures. Although a well-recognized phenomenon, there is still debate about its origins in various materials. The AHE can be either an extrinsic (disorder-related) effect due to spin-dependent scattering of the charge carriers, or an intrinsic effect which can be described in terms of the Berry phase effect in the crystal momentum space (k-space).[52]
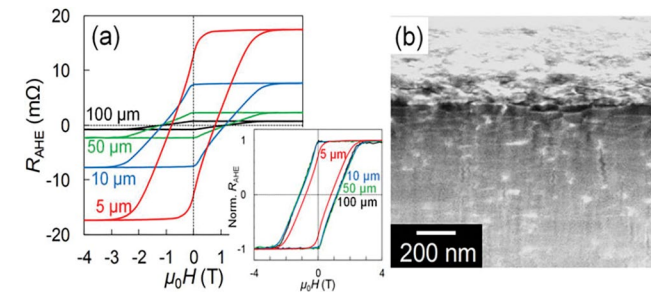
## Anomalous Hall effect (AHE)

**Figure 48** *(a) AHE curves of samples of 100 µm, 50 µm, 10 µm, and 5 µm in thickness. Inset of (a) shows the normalized AHE curves with respect to the saturation. (b) Cross-sectional SEM image of the sample after mechanical polishing.*

## Quantum Hall effect (QHE)

The QHE (or integer quantum Hall effect) is a quantum-mechanical version of the Hall effect, observed in 2D electron systems subjected to very low temperatures and strong magnetic fields, in which the Hall conductance $\sigma$ undergoes quantum Hall transitions leading to a quantization of the Hall conductance.

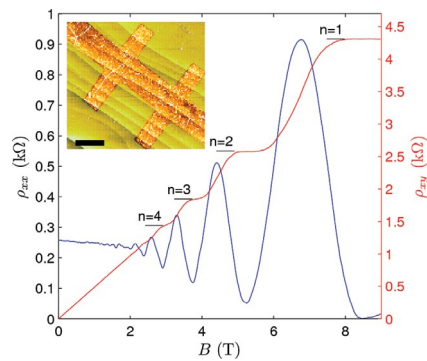**Figure 49**  *QHE in monolayer epitaxial graphene measured at 1.4 K.[53] Hall resistance (red) as a function of magnetic field showing characteristic Hall plateaus, and magnetoresistance $\rho_{xx}$ (blue) showing characteristic oscillations. Inset: Atomic force microscope image of the Hall bar (1.8 μm × 4.6 μm). The scale bar is 2 μm.*

## Harmonic Hall voltage measurements[54]

The harmonic Hall voltage measurement technique has become a standard technique to determine the magnitude of the spin orbital torques. The method uses a Hall bar geometry with an AC current. The sample is oriented such that the external field is either longitudinal or transverse to the current flow. An AC current $I(t) = I_o sin(\omega t)$ is applied, and the first and second harmonic components of the Hall voltage are simultaneously measured using LIAs.
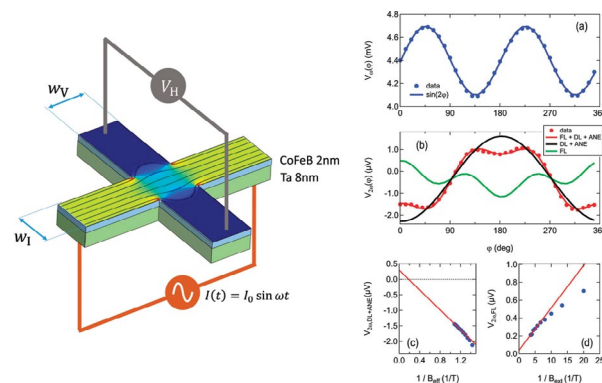
**Figure 50**  *Experimental setup (left) and harmonic Hall voltage measurements (right).*

## Deep-level transient spectroscopy (DLTS)

DLTS is an experimental tool for studying electrically active defects (known as charge carrier traps) in semiconductors. DLTS establishes fundamental defect parameters and measures their concentration in the material. Some of the parameters are considered as defect "fingerprints" used for their identification and analysis.

## Seebeck effect

The Seebeck effect is the buildup of an electric potential across a temperature gradient. A thermocouple measures the difference in potential across a hot and cold end for two dissimilar materials. This potential difference is proportional to the temperature difference between the hot and cold ends. First discovered in 1794 by Italian scientist Alessandro Volta, it is named after the Baltic German physicist Thomas Johann Seebeck, who in 1821 independently rediscovered it. The Seebeck effect can be used to determine if carriers are holes or electrons.

## Other characterization methods complementary to Hall effect measurements

## Hall sensor applications

The emphasis of this book has been using Hall measurement methods to characterize materials, mostly semiconducting materials. In this application the external magnetic field used in the measurement is well characterized and the Hall effect is used to characterize the material.

A Hall sensor turns this on its head. The Hall sensor is a well characterized material that produces a known voltage in a known magnetic field. The Hall sensor is used to determine an external magnetic field. There are numerous applications for Hall sensors. Hall sensors are used with gaussmeters, or teslameters, to measure an external field. A Hall sensor can be used as a proximity sensor to determine if a magnet is near the sensor. Hall sensors are also used as magnetic card readers and have many uses in automotive applications.
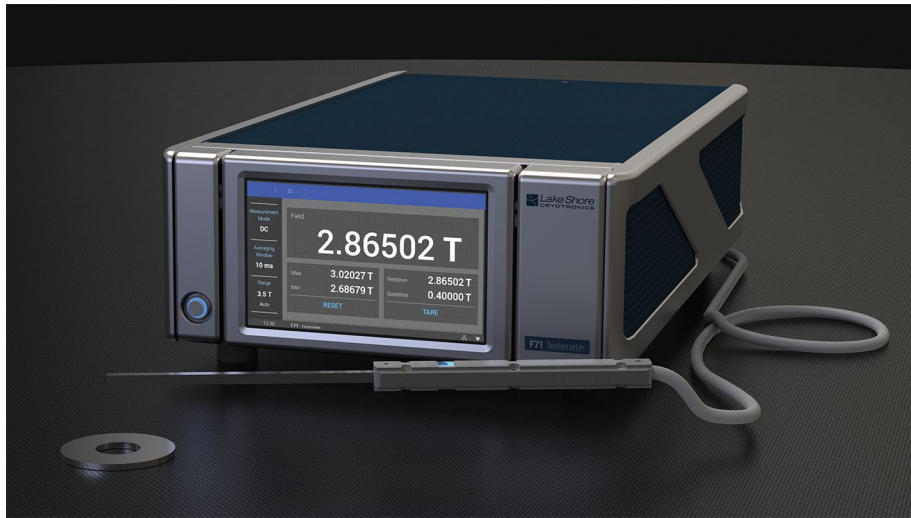


**Figure 51**  *A Hall sensor can be placed at the end of a handled rod, making a Hall probe. This probe is shown connected to a teslameter and taking a measurement of a ring magnet's magnetic field.*

## Instrumentation considerations

### Electrical noise

All electronic measurements must contend with numerous types of noise. Radiated noise from fluorescent lighting, RF signals, and electromechanical devices such as motors can interfere with low level measurements. Johnson noise in resistive elements limits the sensitivity of measurement instruments. Johnson noise voltage is due to the random motion of charged particles resulting from thermal energy. The voltage, $V_{Johnson} = \sqrt{4kT\Delta f}$, where $k$ is Boltzmann's constant, $1.38 \times 10^{-23}$ J/K, $T$ is the absolute temperature in K, and $\Delta f$ is the measurement bandwidth.

### Use of triaxial cable and guards for high resistance measurements

While use of shielded cables is necessary for keeping noise out of the circuit, the shielded cables can have leakage current from the center conductor to the shield conductor. If the voltage across the cable is large enough, a leakage current can reduce the magnitude of the signal reaching the measurement circuit. High resistivity samples can be susceptible to leakage current since a small source current can develop a high voltage across the sample. Using triaxial cables rather than coaxial cables can eliminate leakage current when sample resistivity is high. A g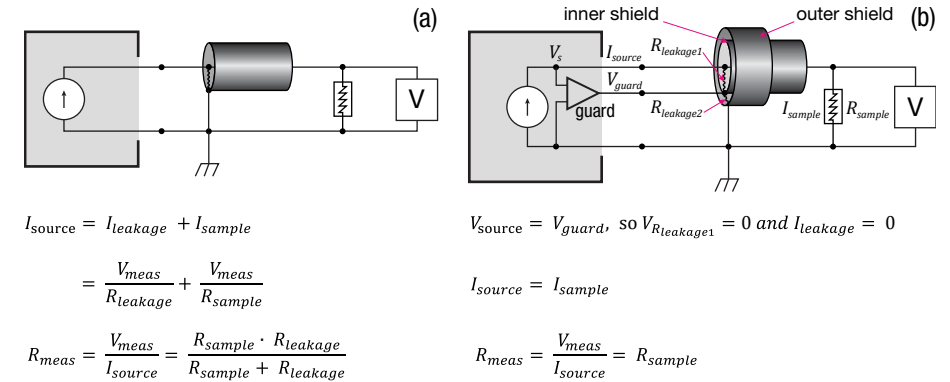uard voltage connected to the output of the source is equivalent to the magnitude of the source output. This voltage is applied to the inner shield of the cable so that the voltage differential across the center conductor and the inner shield is near 0 V. With a negligible voltage difference between the center conductor and the inner shield, no leakage current will flow. See Figure 52. Guarding can also speed up measurements on samples having resistances of 100 MΩ or higher. The high resistance of the sample combined with the capacitance in a shielded cable results in an RC time constant that can take 30 s or longer for voltage measurements to reach a stable value. By using guarding to eliminate the voltage differential across the center conductor and inner shield, the impact of the cable capacitance in the measurement circuit is substantially reduced. The effective RC time constant is reduced, and voltages reach their final value with shorter settling times.



$$I_{source} = I_{leakage} + I_{sample}$$

$$= \frac{V_{meas}}{R_{leakage}} + \frac{V_{meas}}{R_{sample}}$$

$$R_{meas} = \frac{V_{meas}}{I_{source}} = \frac{R_{sample} \cdot R_{leakage}}{R_{sample} + R_{leakage}}$$

$$V_{source} = V_{guard}, \text{ so } V_{R_{leakage1}} = 0 \text{ and } I_{leakage} = 0$$

$$I_{source} = I_{sample}$$

$$R_{meas} = \frac{V_{meas}}{I_{source}} = R_{sample}$$

**Figure 52** *The benefit of guarded connections; (a) an unguarded resistance measurement; (b) same resistance measurement but using guards.*

For high resistivity materials, the sample resistance can have a magnitude in a similar range to the cable leakage resistance. Figure 52a shows that the cable leakage resistance provides a path for leakage current and acts as a parallel shunt to the sample resistance. As a result, the measured resistance is the parallel combination of the cable leakage resistance and the sample resistance. Figure 52b shows how the use of triaxial cables and guarding eliminates errors due to leakage current when testing high resistivity samples. The guard amplifier in the current source is a buffer amplifier with gain of 1. The guard amplifier applies the source voltage to the inner shield of the triaxial cable so that the voltage across the leakage resistance is 0 V. Thus, no current flows through the cable leakage resistance. The current from the guard amplifier flows through the low impedance guard loop and does not flow through the sample resistance. With the triaxial cable and guarding, the sample resistance is properly measured.

## Voltage measurement considerations

Measuring µV and lower Hall voltages requires instruments more sensitive than conventional digital voltmeters. Instruments with nanovolt sensitivity or phase sensitive detectors (lock-in amplifiers) are needed. Johnson noise limits measurement sensitivity and is a function of measurement bandwidth. To achieve DC nanovolt sensitivity, the bandwidth of the measurement instrument must be very low so that the Johnson noise voltage does not overwhelm the Hall voltage. In addition, averaging techniques help eliminate measurement variations due to noise. For DC measurements, measuring the signal over a single or multiple power line cycles averages out fluctuations from power line noise. For AC measurements, the phase sensitive detector's reference signal must stay in phase or locked to the magnet control signal. The detector must also have a high-quality low pass filter to extract the modulated Hall voltage.

When low mobility samples are tested, the high resistivity of the sample creates a high resistance source input to the measurement instrumentation. Minimal voltage measurement error occurs when the source resistance is a small percentage of the input resistance of the measurement instrument. When the sample resistance is high, a specialized high impedance meter is needed to ensure an accurate voltage measurement.

## Ensuring a uniform and stable magnetic field

Whether using the DC Hall measurement method or the AC Hall measurement method, the polarity of the magnetic field needs to be reversed so that the misalignment error voltage can be canceled from the final measurement results. For the DC field method, the magnet must generate a stable and constant magnetic field during the measurement interval. Then the magnet must be switched to the opposite polarity with the same magnitude. For the AC field method, the magnetic field requires a stable oscillating frequency also with equal positive and negative peak values. For electromagnets, a high-stability, low offset voltage bipolar power supply is needed to create a stable magnetic field with equivalent field intensity in either a positive or negative polarity. Also, field uniformity across the sample is essential for generating repeatable measurements. Ensure that the magnet is large enough so the sample will be in the center of the field and not near the edge of the magnet. Conversely, for smaller electromagnets, ensure that the test sample is sufficiently small to reside in a homogeneous region within the electromagnet poles.

## 4-wire measurements

Note that the measurement of resistance is a 4-wire technique, since the current source wires are separate from the voltage measurement wires. This is illustrated schematically in Figure 53. For low resistance (high mobility samples), the test lead resistance is eliminated from the computation of sample resistance. By reversing the polarity of the source current, any thermal voltages due to contacts of dissimilar metals will be eliminated from the computation of resistance.
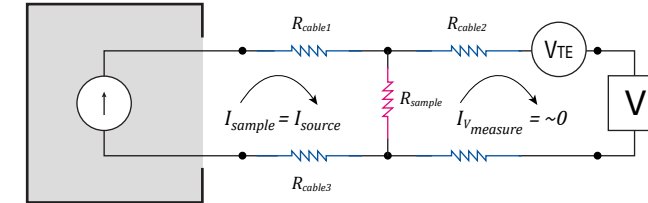


**Figure 53** *4-wire resistance measurement included cable resistance.*

$$V_{cs} = I(R_{cable1} + R_{Sample} + R_{cable2})$$

$$V_{meas}(I_1) = I_1 R_{Sample} + V_{TE}$$

$$V_{meas}(I_2) = I_2 R_{Sample} + V_{TE}$$

$$R_{sample} = \frac{V_{meas}(I_1) - V_{meas}(I_2)}{I_1 - I_2}$$

$V_{CS}$ is the voltage across the current source and includes both the voltage drop across the sample $(R_{sample})$ and the voltage drop across the leads $(R_{cable1} \text{ and } R_{cable2})$.

Typically, in a Hall measurement, the current source is some distance from the sample. It is not unusual to use 3 m long triaxial cables for the connection between the current source and the sample. Even though the cables are guarded, the guards are not perfect and there will be some residual parallel capacitance. This capacitance is in parallel with the sample that has some resistance. When the current source is turned on, the current initially goes to charge the capacitance rather than going through the load. After some time, the capacitor is fully charged, and then all the current goes through the load.

The simplified circuit for the measurement is a current source driving an RC circuit is shown in Figure 54.
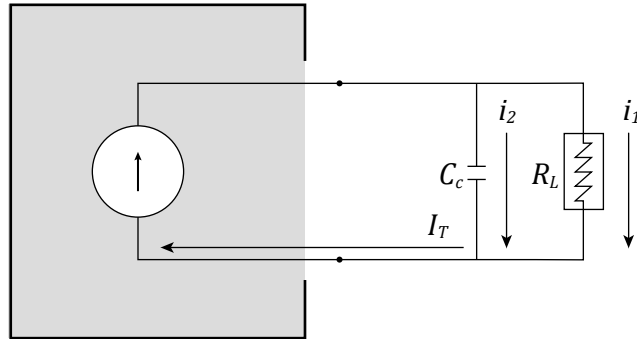


$$i_1 = I_T(1 - e^{-t/R_L C_c}) \qquad i_2 = I_T e^{-t/R_L C_c}$$

*Figure 54* Simplified model of transient effects.

Here $I_T$ is the current from the current source, $R_L$ is the sample resistance, $C_c$ is the capacitance of the cable, $i_1$ is the current through the sample and $i_2$ is the current through the capacitor. To get a valid measurement of $R_L$ it is required to wait for the transient term $(e^{-t/RC})$ to go to a small value. After five time constants the value of $i_2$ is about 0.5% of $I_T$.

To ensure the measurement system provides the best possible measurements, an $I$-$V$ characterization of each contact to the sample should be performed. If the $I$-$V$ characterization of a contact indicates a non-linearity, consider lowering the source current to eliminate the non-linearity in the $I$-$V$ characterization. Also review the quality of the contact preparation.

Another procedure to verify instrumentation and cabling performance is to use a known load as a test sample. A suggested load is a resistor network, as shown in Figure 55, with values approximating the expected resistance of the sample. Insert the resistor network in the sample holder and connect the system cabling to the resistor network's four terminals. Verify that the resistor values are read within the accuracy of the system.
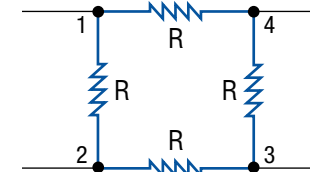


*Figure 55* Resistor test network for testing Hall effect system measurements. Make all resistors of equivalent value; the value should approximate the expected resistance of the test sample.

There are no NIST standards for Hall effect measurements to calibrate a Hall measurement system. The system can be calibrated with precision resistors as explained above. Verify that the resistor values are read within the accuracy of the system. For instance, $R_{13,42}$ (current source on contacts 1 and 3 and voltmeter on contacts 4 and 2) should be $R$. $R_{12,43}$ (current source on contacts 1 and 2 and voltmeter on contacts 4 and 3) should be ¼$R$.

## Commercial Hall measurement system options

Hall effect measurement systems can range from custom systems built from individual instruments to fully integrated hardware/software systems. The choice of test system is based on cost, performance, complexity, and user-skill trade-offs. Table 7 illustrates the trade-offs.

| | Cost | Performance | Assembly and integration complexity | User skill required |
|---|---|---|---|---|
| Fully integrated measurement system | High | High | Low | Low |
| User-configured system | Low | Varied | High | High |
| Measurement controller-based systems | Medium | High | Medium | Medium |

**Table 7** *Instrumentation options for Hall effect measurement systems.*

A turnkey system provides a high level of performance with a complete test system solution. A user of a turnkey system needs minimal skills in working with the test instruments that are built into the system. A turnkey system includes the following:

- Electronics for sourcing, measuring, and signal routing with the appropriate sensitivity, range, resolution, and accuracy to test the type of materials to be studied

- Electromagnet, superconducting magnet, or permanent magnet; associated controller; and power supply to provide sufficient magnetic field strength and uniformity

- Shielded cabling and grounding to minimize the entry of error sources into the system

- Test fixturing to hold the test sample

- Variable temperature options for low and high temperature measurements (if needed)

- A software test environment that enables sequence programming and organization, data collection and visualization, and multiple data analysis capabilities

The Lake Shore Cryotronics 8400 Series Hall measurement system shown in Figure 56 is an example of a turnkey system that provides a complete solution for Hall and resistivity measurements.



**Figure 56** *A turnkey Hall effect measurement system that includes all instrumentation, a magnet, fixturing, and a PC controller.*

The Lake Shore 8400 Series systems can measure carrier mobilities between 1 cm$^2$/V s and $1 \times 10^6$ cm$^2$/V s using the DC field measurement methodology. Using AC field techniques, carrier mobility measurements can be extended down to near $1 \times 10^{-3}$ cm$^2$/V s to test very low mobility materials.

The 8400 Series provides DC magnetic field intensities up to 2.25 T (22.5 kOe) and AC field intensities up to 1.31 T (13.1 kOe) to characterize Hall voltages for a wide range of materials. The system can make resistance measurements on low resistance materials down to 0.5 mΩ, and optional system configurations enable measurements on high resistance materials up to 200 GΩ.

A further advantage of a turnkey system is that several additional challenges have been solved, such as options for keeping the magnet temperature controlled to maintain a stable, uniform field across the sample. In addition, a liquid nitrogen cryostat option enables fixed point testing at 77 K. Other options provide continuously variable temperature measurements between 15 K and 400 K using cryogen-free closed cycle refrigeration (CCR), and ovens for testing samples at temperatures up to 1273 K. DC field Hall measurements to field strengths of 2.5 T (25 kOe) are possible in the Model 8425 cryogenic probe station equipped with a superconducting magnet shown in Figure 57. This system also provides a vacuum-controlled cryogenic chamber to test samples both at low temperature (~15 K) and in the absence of any charge carriers in the atmosphere. With the 8425 cryogenic probe station-based system, vacuums as low as $5 \times 10^{-7}$ Torr can be maintained.



**Figure 57** *Cryogenic sample holder enables testing samples at temperatures as low as 15 K and under a vacuum.*

The 8400 Series Hall measurement systems have options for gate bias control and a fixture to photoexcite samples either directly with a laser or indirectly through a fiber optic cable, which allows exposure of the sample to different light wavelengths. Thus, a turnkey system, such as an 8400 Series Hall measurement system, can perform an extensive range of measurements over a wide range of temperatures and other conditions to enable testing of a wide variety of materials. The system conveniently minimizes and compensates for the misalignment voltage offsets, thermal voltage offsets, and noise voltages that can interfere with the Hall voltage and the sheet resistivity measurements. The system also performs all computations and presents data in multiple formats to simplify analysis and material characterization.

A user-configured system is a low-cost option, but such a system requires a highly skilled and knowledgeable user. A user-configured system will consist of the following:

**User-configured systems**

■ Individual instruments for sourcing and measuring; a switch control system may be included for automated signal routing

■ A magnet and its control instrumentation; depending on the flexibility of the system, the magnet can be an electromagnet, superconducting magnet, or permanent magnet

■ Sample holder — the sample holder may be a cryogenic or high temperature chamber to allow testing at low and high temperatures respectively, and testing under vacuum

■ Cabling for instrument and sample interconnection

■ Software for data collection and analysis

The developer of a user-configured system must also trade off the development time to define, construct, test, and troubleshoot the system compared with the higher cost of a turnkey system. All the work needed to develop, test, and validate performance has been completed in an integrated turnkey system, ensuring accurate and reproducible measurement results for a wide range of materials. A user-configured system does offer the advantage of testing new materials, which require measurements that may be outside the range of commercially-available turnkey systems; however, the custom system may make it more difficult for measurement results to be repeated and verified by other researchers using their independently configured systems.

**Measurement controller-based systems**

A measurement controller provides an intermediate stage of system integration by including instrumentation, control, and analysis in one physical package. A measurement controller-based system includes:

- The measurement controller, which contains:

    - Electronics for sourcing, measuring, and signal routing

    - Control, calculation, analysis, and display algorithms

- A magnet and its control instrumentation

- Cryostat and/or oven and control instrumentation if variable temperature measurements are required

- Sample holder

The measurement controller reduces the assembly and integration complexity compared to a user-configured system. The user still needs to focus on sample fixturing, magnet, and temperature option selection. The measurement controller resolves the measurement challenges, provides appropriate instrument control settings, and provides computation results and analytical information. These capabilities considerably simplify the user's integration and assembly task and help ensure that results can be independently repeated. A Lake Shore Cryotronics Hall measurement controller is shown in Figure 58.



*Figure 58* *An M91 FastHall™ measurement controller containing all the measurement instruments and software for making Hall effect and resistivity measurements.*

The Lake Shore Cryotronics Hall measurement controller is also available as the primary instrument in a fully integrated, high precision tabletop system, named the FastHall™ Station.

This station, which allows for less experimental setup, has all the necessary components and cabling to provide a range of measurement capabilities, including sample resistances up to 1 GΩ and low mobility measurements down to 0.01 cm²/V s.

In addition to the measurement controller, the tabletop system includes:

- 1 T permanent magnet

- A high-performance sample holder

- A sample card starter kit (including both solder and prober pin-style cards)

- Windows® computer with monitor

- Application/analysis software for automated Hall measurement data collection and analysis; creating data tables, charts, and reports; and outputting .csv data files for further analysis

- Hall application packs and a software development kit for measurement customization

The light-tight system offers an enclosed, electronically shielded, low-noise sample space with triaxial connections with a driven guard all the way to sample. The prober pin-style cards included with the station allow a researcher to mount samples without requiring contact pad soldering. You can load a sample and immediately begin running van der Pauw or Hall bar measurements. A parameter optimization function automatically selects the best parameters for optimum results, and software offers complete control of Hall measurement operations, whether you want to customize, start, or step through measurement sequences, as well as chart, log, and organize the results.

As standard, the tabletop station supports room temperature measurements. However, to convert the standard station into a cryogenically cooled sample space, an $LN_2$ option can be specified.

Also available: a gate bias option, which includes a low-noise DC current/voltage source instrument for conducting Hall measurements with a gate bias applied.



*Figure 59* *The tabletop FastHall™ Station, which includes the M91 measurement controller.*

## Summary

Hall effect measurements are fundamental for semiconductor material characterization and determine important parameters such as charge carrier concentration, material resistivity, charge carrier mobility, and other material properties. The Hall effect is a very common measurement. The simplicity can often be a disadvantage. The nuances, which are present in any measurement technique are not always studied or taken seriously. It is our hope that this guide will help users, from the novice to seasoned expert, understand some of the subtleties of Hall measurements.

"Mathematics began to seem too much like puzzle solving. Physics is puzzle solving, too, but of puzzles created by nature, not by the mind of man."
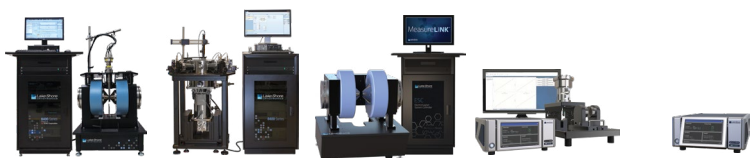
– Maria Goeppert-Mayer

## Hall effect measurement system options

Lake Shore Cryotronics offers a wide range of Hall measurement solutions from turnkey Hall measurement systems to instrument-only measurement controllers. Temperature options are available for variable temperature measurements from <4 K up to 1273 K depending on the system type. Magnet options available include electromagnet, superconducting, and permanent magnet types. The M91 FastHall™ measurement controller instrument performance in a system is dependent on the magnet and the sample fixturing used.



| Description | Electromagnet Hall System | Probe station Hall system | MeasureReady™ MCS-EMP with 7- or 4-inch magnet and FastHall measurement module | MeasureReady™ FastHall Station | MeasureReady™ FastHall measurement controller |
|---|---|---|---|---|---|
| Model | 8404/8407 | 8425 | MCS-EMP-7 or MCS-EMP-4 and EMP-MM-FASTHALL | HMS-TT-MAN | M91/M91-HR |
| Carrier mobility measurement range | DC field: 1 cm²/V s to 1 × 10⁶ cm²/V s  AC field: 1 × 10⁻³ cm²/V s to 1 × 10⁶ cm²/V s | 1 cm²/V s to 1 × 10⁶ cm²/V s | DC field: 1 cm²/V s to 1 × 10⁶ cm²/V s  AC field: NA | 1 × 10⁻² cm²/V s to 1 × 10⁶ cm²/V s | 1 × 10⁻³ cm²/V s to 1 × 10⁶ cm²/V s |
| Resistance measurement range | Standard: 0.5 mΩ to 10 MΩ  Optional high resistance configuration: 10 MΩ to 200 GΩ | Standard: 0.5 mΩ to 10 MΩ  Optional high resistance configuration: 10 MΩ to 100 GΩ | Standard: 0.5 mΩ to 10 MΩ  Optional high resistance configuration: 10 MΩ to 200 GΩ | 10 mΩ to 1 GΩ | Standard: 10 mΩ to 10 MΩ  Optional high resistance configuration: 10 MΩ to 200 GΩ |
| Current source range | ±1 pA to ±100 mA | ±1 pA to ±100 mA | ±10 pA to ±100 mA | ±10 pA to ±100 mA | ±10 pA to ±100 mA |
| Current measurement range | ±1 pA to ±100 mA | ±1 pA to ±100 mA | ±1 pA to ±100 mA | ±1 pA to ±100 mA | ±1 pA to ±100 mA |
| Voltage source range | NA | NA | ±1 µV to ±10 V | ±1 µV to ±10 V | ±1 µV to ±10 V |
| Voltage measurement range | ±100 nV to ±100 V | ±100 nV to ±100 V | ±1 µV to ±10 V | ±1 µV to ±10 V | ±1 µV to ±10 V |

| Description | Electromagnet Hall System | Probe station Hall system | MeasureReady™ MCS-EMP with 7- or 4-inch magnet and FastHall measurement module | MeasureReady™ FastHall Station | MeasureReady™ FastHall measurement controller |
|---|---|---|---|---|---|
| Model | 8404/8407 | 8425 | MCS-EMP-7 or MCS-EMP-4 and EMP-MM-FASTHALL | HMS-TT-MAN | M91/M91-HR |
| Maximum voltage | ±100 V | ±100 V | ±10 V | ±10 V | ±10 V |
| AC field frequencies | 0.05 Hz, 0.1 Hz | NA | NA | NA | NA |
| Room temperature DC magnetic field intensities | 7 in: 2.10 T, 2.25 T  4 in: 1.35 T, 1.67 T | 2.0 T | 7 in: 2.10 T, 2.25 T  4 in: 1.35 T, 1.67 T | 1.0 T | NA |
| Room temperature AC field intensities | 7 in: 1.20 T, 1.31 T  4 in: 0.95 T, 1.18 T | NA | 7 in: 1.20 T, 1.31 T  4 in: 0.95 T, 1.18 T | NA | NA |
| Variable temperature DC magnetic field intensities | 7 in: 0.89 T, 1.45 T  4 in: 0.88 T | ±2 T | 7 in: 0.89 T, 1.45 T  4 in: 0.88 T | NA | NA |
| Variable temperature AC magnetic field intensities | 7 in: 0.63 T, 0.69 T  4 in: 0.62 T | NA | 7 in: 0.63 T, 0.69 T  4 in: 0.62 T | NA | NA |
| Closed cycle refrigeration temperature range | Optional: 15 K to 400 K | Standard: 10 K to 400 K | Optional: 15 K to 400 K | NA | NA |
| Oven temperature range | Optional: room temperature to 1273 K | NA | Optional: room temperature to 1273 K | NA | NA |
| Highest vacuum | NA | Standard: 1 × 10⁻⁵ Torr  Optional: 5 × 10⁻⁷ Torr | NA | NA | NA |
| Maximum sample size | Standard: 10 mm × 10 mm × 3 mm  Optional: 50 mm diameter × 3 mm | 51 mm diameter | Standard: 10 mm × 10 mm × 3 mm  Optional: 50 mm diameter × 3 mm | 10 mm × 10 mm × 3 mm | NA |
| DC field Hall measurement speed, typical | 180 s | 600 s | 180 s | 10 s | 10 s |
| AC field Hall measurement speed, typical | 3600 s | NA | NA | NA | NA |

# References

1. E. H. Hall, "On a New Action of the Magnet on Electric Currents," American Journal of Mathematics 2 (3), 287 – 292 (1879).

2. ASTM International, "ASTM-F76," edited by ASTM.

3. D.K. Schroder, Semiconductor Material and Device Characterization. (Wiley, 1998).

4. Van der Pauw, "1958 Van der Pauw (Philips Res Rep) A method of measuring specific resistivity and Hall effect of discs of arbitrary shape."

5. D. C. Look, Electrical Characterization of GaAs Materials and Devices. (Wiley, New York, 1989).

6. J. Volger, "Note on the Hall Potential Across an Inhomogeneous Conductor," Physical Review 79 (6), 1023 – 1024 (1950).

7. J. Haeusler and H. J. Lippmann, "Hallgeneratoren mit kleinem linearisierungsfehler," Solid-State Electronics 11 (1), 173 – 182 (1968).

8. Serge Jandl, K. D. Usadel, and Gaston Fischer, "Resistivity measurements with samples in the form of a double cross," Review of Scientific Instruments 45 (11), 1479 – 1480 (1974).

9. Ronald Chwang, B. J. Smith, and C. R. Crowell, "Contact size effects on the van der Pauw method for resistivity and Hall coefficient measurement," Solid-State Electronics 17 (12), 1217 – 1227 (1974).

10. H.J. van Daal, "Mobility of charge carriers in silicon carbide," Philips research reports Suppl. 3, 1 – 92 (1965).

11. G. De Mey, "Potential Calculations for Hall Plates," Advances in Electronics and Electron Physics 61 (1983).

12. G. De Mey, "Influence of sample geometry on Hall mobility measurements," Arch. Electron. Uebertragungstech. 27, 309 – 313 (1973).

13. H. K. Henisch, Semiconductor Contacts: an approach to ideas and models. (Clarendon Press, 1984).

14. T. C. Shen, G. B. Gao, and H. Morkoç, "Recent Developments in ohmic contacts for III-$V$ compound semiconductors," J. Vac. Soc. Technol. B 10 (1992).

15. A. M. Hermann and J. S. Ham, "Apparatus for the Measurement of the Hall Effect in Semiconductors of Low Mobility and High Resistivity," Review of Scientific Instruments 36 (11), 1553 – 1555 (1965).

16. D. Parker and J. Yahia, "AC Hall Measurements in Crystals of Strontium Titanate from 190 to 500K: Dependence of Hall Mobility on Charge-Carrier Density," Physical Review 169 (3), 605 – 609 (1968).

17. Hermann von Helmholtz, "Ueber einige Gesetze der Vertheilung elektrischer Ströme in körperlichen Leitern mit Anwendung auf die thierisch-elektrischen Versuche" [Some laws concerning the distribution of electrical currents in conductors with applications to experiments on animal electricity]," Annalen der Physik und Chemie 89 (6), 211 – 233 (1853).

18. Léon Charles Thévenin, "Extension de la loi d'Ohm aux circuits électromoteurs complexes [Extension of Ohm's law to complex electromotive circuits]," Annales Télégraphiques 10, 222 – 224 (1883).

19. Hans Ferdinand Mayer, "Ueber das Ersatzschema der Verstärkerröhre [On equivalent circuits for electronic amplifiers]," Telegraphen- und Fernsprech-Technik 15, 335 – 337 (1926).

20. Edward Lawry Norton, 1926.

21. Lars Onsager, "Reciprocal Relationships in Irreversible Processes I," Phys Rev 37 (1931).

22. H. H. Sample, W. J. Bruno, S. B. Sample, and E. K. Sichel, "Reverse-field reciprocity for conducting specimens in magnetic fields," Journal of Applied Physics 61 (3), 1079 – 1084 (1987).

23. Fast Hall effect measurement system Jeffrey Lindemuth, 9797965, USA (2017).

24. K.S. Suresh Kumar, Electric Circuits and Networks. (Pearson Eduxation India, India, 2009).

25. P. J. A. Munter, "A low-offset spinning-current Hall plate," Sensors and Actuators A: Physical 22 (1–3), 743 – 746 (1990).

26. P. J. A. Munter, "Electronic circuitry for a smart spinning-current Hall plate with low offset," Sensors and Actuators A: Physical 27 (1–3), 747 – 751 (1991).

27. S. Bellekom and L. Sarro, presented at the Solid State Sensors and Actuators, 1997. TRANSDUCERS '97 Chicago., 1997 International Conference on, 1997 (unpublished).

28. R. Steiner, Ch Maier, A. Hàberli, F. P. Steiner, and H. Baltes, "Offset reduction in Hall devices by continuous spinning current method," Sensors and Actuators A: Physical 66 (1–3), 167 – 172 (1998).

29. E.H. Putley, The Hall effect and semi-conductor physics. (Dover Publications, 1960).

30. D. C. Look and P. C. Colter, "Electrical properties of low-compensation GaAs," Physical Review B 28 (2), 1151 – 1153 (1983).

31. D. C. Look, "Statistics of multicharge centers in semiconductors: Applications," Physical Review B 24 (10), 5852 – 5862 (1981).

32. Nan Wang and Yang Qi, "Enhanced transport properties of Bi thin film by preferential current flow pathways in low angle grain boundaries," Vacuum 169, 108874 (2019).

33. G. Brauer, W. Anwand, W. Skorupa, J. Kuriplach, O. Melikhova, C. Moisson, H. von Wenckstern, H. Schmidt, M. Lorenz, and M. Grundmann, "Defects in virgin and N+-implanted ZnO single crystals studied by positron annihilation, Hall effect, and deep-level transient spectroscopy," Physical Review B 74 (4), 045208 (2006).

34. J. S. Kim, D. G. Seiler, and W. F. Tseng, "Multicarrier characterization method for extracting mobilities and carrier densities of semiconductors from variable magnetic field measurements," Journal of Applied Physics 73 (12), 8324 – 8335 (1993).

35. D. C. Look, C. E. Stutz, and C. A. Bozada, "Analytical two-layer Hall analysis: Application to modulation-doped field-effect transistors," Journal of Applied Physics 74 (1), 311 – 314 (1993).

36. Z. Dziuba and M. Gorska, "Analysis of the electrical-conduction using an iterative method," J. Phys. III 2 (7), 99 – 110 (1992).

37. Yu-Ming Lin, Christos Dimitrakopoulos, Damon B. Farmer, Shu-Jen Han, Yanqing Wu, Wenjuan Zhu, D. Kurt Gaskill, Joseph L. Tedesco, Rachael L. Myers-Ward, Charles R. Eddy Jr., Alfred Grill, and Phaedon Avouris, "Multicarrier transport in epitaxial multilayer graphene," Applied Physics Letters 97 (11), 112107 (2010).

38. W. A. Beck and J. R. Anderson, "Determination of electrical transport properties using a novel magnetic field-dependent Hall technique," J. Appl. Phys. 62 (2), 541 – 554 (1987).

39. M. Myronov, S. Kiatgamolchai, O. A. Mironov, V. G. Kantser, E. H. C. Parker, and T. E. Whall, "Mobility spectrum computational analysis using a maximum entropy approach," Phys. Rev. E 66 (3) (2002).

40. J. P. Hague, D. Chrastina, and D. R. Leadley, "Application of Bryan's algorithm to the mobility spectrum analysis of semiconductor devices," J. Appl. Phys. 94 (19), 6583-6590 (2003).

41. M. Jarrell and J. E. Gubernatis, Physics Reports 269, 133 (1996).

42. D. Seymeour, J. Antoszewski, L. Faraone, J. R. Meyer, and C. A. Hofman, "Magneto-transport characterization using quantitative mobility-spectrum analysis," J. Electron. Mat. 24 (9), 1255 – 1262 (1995).

43. J. R. Meyer, I. Vurgaftman, C. A. Hofman, D. Redfern, J. Antoszewski, L. Faraone, and J. R. Lindemuth, "Improved quantitative mobility spectrum analysis for Hall characterization," J. Appl. Phys. 84 (9), 966 – 973 (1998).

44. Gang Du, J. R. Lindemuth, B. C. Dodrill, R. Sandhu, M. Wojtowicz, Mark S. Goorsky, I. Vurgaftman, and J. R. Meyer, "Characterizing Multi-Carrier Devices with Quantitative Mobility Spectrum Analysis and Variable Field Hall Measurements," Japanese Journal of Applied Physics 41, 1055 (2002).

45. H. I. Zhang and J. Callaway, "Energy-Band Structure and Optical Properties of GaSb," Physical Review 181 (3), 1163 – 1172 (1969).

46. V. W. L. Chin, "Electron mobility in GaSb," Solid-State Electronics 38 (1), 59 – 67 (1995).

47. M. K. Hudait, Y. Lin, P. M. Sinha, J. R. Lindemuth, and S. A. Ringel, "Carrier compensation and scattering mechanisms in Si-doped $InAs_yP_{1-y}$ layers grown on InP substrates using intermediate $InAs_yP_{1-y}$ step-graded buffers," Journal of Applied Physics 100 (6), 063705 – 063709 (2006).

48. S. Monaghan, F. Gity, R. Duffy, G. Mirabelli, M. McCarthy, K. Cherkaoui, I. M. Povey, R. E. Nagle, P. K. Hurley, J. R. Lindemuth, and E. Napolitani, presented at the 2017 Joint International EUROSOI Workshop and International Conference on Ultimate Integration on Silicon (EUROSOI-ULIS), 2017 (unpublished).

49. R. Srivastava, A. Saxena, and S. Ingole, "n-Type iron pyrite $(FeS_2)$ thin-films obtained at different sulfur vapor pressures," Chalcogenide Letters 14 (6), 227 – 237 (2017).

50. Chanyoung Yim, Niall McEvoy, Sarah Riazimehr, Daniel S. Schneider, Farzan Gity, Scott Monaghan, Paul K. Hurley, Max C. Lemme, and Georg S. Duesberg, "Wide Spectral Photoresponse of Layered Platinum Diselenide-Based Photodiodes," Nano Letters 18 (3), 1794 – 1800 (2018). https://pubs.acs.org/doi/10.1021/acs.nanolett.7b05000. Further permissions related to this excerpted material should be directed to the ACS.

51. Bing Zhao, Dmitrii Khokhriakov, Yang Zhang, Huixia Fu, Bogdan Karpiak, Anamul Md Hoque, Xiaoguang Xu, Yong Jiang, Binghai Yan, and Saroj P Dash, "Observation of Spin Hall Effect in Weyl Semimetal $WTe_2$ at Room Temperature," arXiv preprint arXiv:1812.02113 (2018).

52. Takahiro Yomogita, Nobuaki Kikuchi, Satoshi Okamoto, Osamu Kitakami, Hossein Sepehri-Amin, Tadakatsu Ohkubo, Kazuhiro Hono, Keiko Hioki, and Atsushi Hattori, "Detection of elemental magnetization reversal events in a micro-patterned Nd-Fe-B hot-deformed magnet," AIP Advances 9 (12), 125052 (2019).

53. Xiaosong Wu, Yike Hu, Ming Ruan, Nerasoa K. Madiomanana, John Hankinson, Mike Sprinkle, Claire Berger, and Walt A. de Heer, "Anomalous quantum Hall effect in epitaxial graphene," arXiv preprint arXiv:0908.4112 (2009).

54. Lukas Neumann and Markus Meinert, "Influence of the Hall-bar geometry on harmonic Hall voltage measurements of spin-orbit torques," AIP Advances 8 (9), 095320 (2018).

### About the Author

Dr. Jeffrey Lindemuth is a Senior Scientist with Lake Shore. He received his BSc in Physics from Penn State University and his PhD in High Energy Physics from the College of William and Mary in 1982, where his research concentrated on the study of weak and strong interactions through the measurements of exotic atom x-rays. Before Lake Shore, Dr. Lindemuth was with EG&G Princeton Applied Research, concentrating on computer-aided measurements and data analysis for electrochemistry, optical spectroscopy, fiber optics, magnetic materials, and high-speed electronics. He later became Director of R&D for the company. Since joining Lake Shore in 1993, his focus has been in the development of magnetic measurement systems, including VSMs and AC susceptibility measurements as well as Hall systems and data analysis. In addition, Dr. Lindemuth performs application training, working closely with customers to help them better understand the measurements obtained from their VSM and Hall systems. He is widely recognized as an expert in instrumentation and methods for Hall measurements, particularly in semiconductor materials.

## Lake Shore
### CRYOTRONICS